RECEIVED
LAWRENCE
RADIATION LABORATORY

LIBRARY AND
DOCUMENTS SECTION

LBL-134

C.1

ON THE DEFORMATION INDUCED MARTENSITE TRANSFORMATION IN Fe-Ni AND Fe-Ni-Cr SINGLE CRYSTALS

Glen A. Stone
(M. S. Thesis)

September 1971

AEC Contract No. W-7405-eng-48

For Reference

Not to be taken from this room

LAWRENCE BERKELEY LABORATORY
UNIVERSITY OF CALIFORNIA
BERKELEY

LBL-134

C.1

DISCLAIMER

This document was prepared as an account of work sponsored by the United States Government. While this document is believed to contain correct information, neither the United States Government nor any agency thereof, nor the Regents of the University of California, nor any of their employees, makes any warranty, express or implied, or assumes any legal responsibility for the accuracy, completeness, or usefulness of any information, apparatus, product, or process disclosed, or represents that its use would not infringe privately owned rights. Reference herein to any specific commercial product, process, or service by its trade name, trademark, manufacturer, or otherwise, does not necessarily constitute or imply its endorsement, recommendation, or favoring by the United States Government or any agency thereof, or the Regents of the University of California. The views and opinions of authors expressed herein do not necessarily state or reflect those of the United States Government or any agency thereof or the Regents of the University of California.

0 0 0 0 3 6 0 5 5 5 6

Table of Contents

Abstract v

I. Introduction 1

II. Experimental Procedures 3

A. Material Preparation 3

B. Lattice Parameter Measurements 4

C. Mechanical Property Measurements 5

D. Metallography 6

E. Identification of the Martensite Variants of the Orientation Relationship 6

F. Volume Fraction Measurements of Each K-S Variant 8

III. Experimental Results 11

A. Mechanical Properties and Microstructure 11

1. Fe-34.5 w/o Ni Alloy 11

2. Fe-15 w/o Ni-15 w/o Cr Alloy 13

B. Experimentally Observed Variants of the Orientation Relationship 14

1. Fe-34.5 w/o Ni Alloy 14

2. Fe-15 w/o Ni-15 w/o Cr Alloy 15

IV. Discussion 17

A. Plastic Flow in Face Centered Cubic Austenite 17

B. Effect of Crystal Orientation on the Martensite Transformation 23

1. Fe-34 w/o Ni Alloy 23

2. Fe-15 w/o Ni-15 w/o Cr Alloy 25

V. Summary and Conclusions 29

Acknowledgments 32

Appendix 33

A. Method of X-ray Volume Fraction Measurements 33

B. Computer Program for Mechanical Property Data Reduction and Cal Comp Plotting 35

C. Two Surface Analysis Calculations of Martensite Habit Plane with Computer Program 41

References 44

Figure Captions 54

ON THE DEFORMATION INDUCED MARTENSITE TRANSFORMATION IN Fe-Ni AND Fe-Ni-Cr SINGLE CRYSTALS

Glen A. Stone

Inorganic Materials Research Division, Lawrence Berkeley Laboratory and Department of Materials Science and Engineering, College of Engineering; University of California, Berkeley, California

ABSTRACT

The deformation induced martensite transformation has been studied on Fe-34.5 w/o Ni and Fe-15 w/o Ni-15 w/o Cr single crystal alloys as a function of crystal orientation. Specimens were tested with tensile axes of ⟨123⟩ (easy glide) and ⟨112⟩ (duplex slip) and the resulting transformation was studied by x-ray and electronmicroscopy techniques. A method is presented showing how the specific Kudjumov-Sachs (K-S) variants formed can be identified in the crystal. A method to calculate the habit plane from a single trace of an electronmicrograph is shown. This method requires accurate habit plane data which was obtained by the conventional two surface analysis method.

It was found for Fe-34.5 w/o Ni alloys crystals oriented for easy glide that a single K-S variant was favored. For duplex slip, two symmetrical variants appeared which contained the majority of the martensite formed. The martensite produced as a result of plastic deformation, formed on a $\{111\}_f$ plane of zero shear adjacent to the slip plane. The K-S variant formed was always associated with the operating slip vector in the austenite. The Fe-15 w/o Ni-15 w/o Cr alloy crystals also produced a transformation product of a specific K-S variant for easy glide crystals and a symmetrical K-S pair for duplex slip crystals. However, for this alloy, the K-S variant was always that containing the $\{111\}_f$ slip plane and $\langle 110 \rangle_f$ slip vector.

Hexagonal close packed ε martensite was observed in all Fe-15 w/o Ni-15 w/o Cr alloy crystals tested above 242°K. The crystals tested at 242°K contained no α martensite. The ε phase was always associated with the active slip systems in the crystals tested.

0 0 0 0 3 6 0 0 3 3 8

I. INTRODUCTION

The objective of this paper is to study the role of applied stress on the martensite transformation of single crystal Fe-Ni and Fe-Ni-Cr alloys. Of particular interest: What is the effect of orientation on the transformation process? What variants are favored in the transformation as a function of crystal orientation and how can this information aid in forming ideas as to the formation and configuration of the martensite embryo? The primary difficulty with the present state of knowledge is a lack of real understanding as to the nature of the martensite embryo. The results to be presented here have not solved the critical problem of martensite embryo, but do offer a fresh experimental approach to the nucleation problem, and hopefully these data can be extended to more sophisticated analyses. From a practical point of view, a better understanding of the stress-strain induced martensite transformation will lead to better control of metallurgical variables during material processing.

The martensite nucleation problem has been reviewed by Kaufman and Cohen[1] and more recently by Magee.[2] These reviews offer a comprehensive statement of thermodynamics and mechanistic parameters involved in the martensite nucleation theories and therefore will not be presented in this thesis. The possible embryo configurations which have been proposed and discussed in the literature over the years are reviewed by Russell.[3] A model showing the effect of stress on the Ms temperature has been developed by Patel and Cohen.[4] This model has recently been applied by Goodchild, et al.[5] to estimate the effect of stress on the formation of specific martensite variants in textured 301 and 305 stainless steel alloys.

In this study it is shown that specific variants of both the ε and α martensite are strongly related to the state of stress in the crystal. In particular the distribution of the martensite variants present can be correlated to the slip systems operating in the crystal. Quantitative volume fraction measurements, of each variant present, have shown that 80% of the martensite present in crystals orientated for easy glide occurs on only one variant of the Kudjumov-Sachs (K-S) orientation relationship. For duplex slip the majority of martensite present is divided among two specific variants of the orientation relation. The balance of martensite observed for both single and duplex slip specimens is related to adjacent {111} austenite planes which have slipped due to accommodation of martensite generated by the primary slip systems. In addition to data related to the main topic of this thesis, precision lattice parameter measurements of the γ and α phases and a discussion of the mechanical properties will be presented for the two alloys studied.

II. EXPERIMENTAL PROCEDURES

A. Material Preparation

Two single crystal alloys, Fe-34.5% Ni (alloy 1) and Fe-15% Ni-15% Cr (alloy 2) were selected for this study. The crystals are 32 mm in diameter by 160 mm long, and were grown by Advanced Materials Research and Development Laboratory of Pratt and Whitney Aircraft.[6] Alloy 1 is a ferromagnetic austenite which has a high stacking fault energy, and thus tends to form a plate-like b.c.c. α martensite. Alloy 2 is a paramagnetic austenite which has a fairly low stacking fault energy (20-30 ergs/cm^2; estimated from data of Breedis[7]) which forms a lath type morphology containing hexagonal close packed ε and α martensite. Keeping the experimental objectives in mind, the two alloys will allow differences in the distribution of the martensite variants to be observed. The correlation of these differences to slip in the crystals may help to visualize possible dislocation interactions which produce the marked difference in martensite morphology of these alloys and insight into the nucleation process.

The crystals were homogenized at 1200°C for 72 hours. Sheets 2.5 mm thick were cut from the crystals, the face of the sheet being the $(111)_f$ (symbols f, b, and h will be used to subscript Miller indices for the face center cubic, body center cubic and hexagonal close-packed crystal structures respectively). The long axis of the as grown crystal is within 5° of the $[001]_f$. The sheet is therefore elliptical with the major axis 65 mm and the minor axis 32 mm. All specimens used in this study were machined from three adjacent slabs of each alloy.

The single crystal slabs were cut from the large crystal with a Norton abrasive disk no. A90 R0R30. The cutting was performed under a

continuous flow of kerosene at 6000 RPM. The slabs were surface ground using 0.0002 mm steps in the grinding operation. The final specimen configuration is shown in Fig. 1. The tensile specimens were electropolished, removing a minimum of 0.25 mm of material from the surface.

The electropolishing solution used for alloy 1 was 87.5g CrO_3 crystals, 473 ml of acetic acid and 25 ml of distilled water. The specimens were polished at 10 volts, maintaining the temperature at 25°C. The rate of material removed was between 0.06 and 0.10 mm/hour, producing a mirror finish with a few scattered pits. Alloy 2 was electropolished with 15% $HClO_3$(60%), 85% acetic acid at 8 volts, maintaining a temperature of 15°C. The rate of removal was 0.10 to 0.15 mm/hour, producing again a uniform mirror finish. Both alloys were electropolished using a stainless steel beaker for a cathode and the solution was stirred very slowly with a magnetic stirrer.

The initial orientation of the crystals for machining and a recheck of each tensile specimen before testing was performed using the Laue back reflection method. Some splitting of Laue spots was observed for alloy 2, whereas alloy 1 exhibited sharp and symmetrical reflections. The final orientation of each crystal was measured by locating the three $\{002\}_f$ peaks with a Schulz pole figure goniometer, which is mounted on a Norelco diffractometer. All orientation measurements are estimated to be accurate to 1 degree.

B. Lattice Parameter Measurements

Powders for austenite lattice parameter measurements were made by filing with a jewlers file at room temperature (the M_d temperature for both alloys is below room temperature). The powders were

capsulated in quartz under vacuum and annealed for 2 hours at 850°C. The powders were mixed with a silicon standard (a_0 = 5.43054)[8] and film exposed for both high and low angle lines, using a Guinier-Jagodzinski double cylinder camera[9] with FeKα_1, monochromatic radiation. Powders for martensite lattice parameters were made by filing at -196°C, capsulated and annealed for 4 days at 275°C. Using a silicon standard, films were exposed in a 114.8 mm radius Debye-Scherrer camera, using FeKα radiation. The 275°C anneal caused the $\varepsilon \rightarrow \gamma$ transformations to proceed in alloy 2; therefore it was not possible to measure the lattice parameters of ε martensite, which were observed in alloy 2 by optical and x-ray experiments.

Measurements were made from the films by the author and one independent observer. The combined data of these measurements were treated by Fortran IV computer programs POWCOR and LCLSQ.[10] These programs correct the observed data for any film instabilities, and linear shifts in measurements based on the silicon standard lines. The data is then treated to a least squares regression analysis, enumerating the best possible value of a_0 for each set of input data. The resulting lattice parameter measurements are presented in Table I. The accuracy given in Table I is one standard deviation. Additional information on the lattice parameters of Fe-Ni and Fe-Ni-Cr alloys maybe found in the literature.[11,12]

C. Mechanical Property Measurements

All tensile tests were performed with an Instron Model TT-M testing machine. The specimens were gripped, using block type grips with universal action to aid in critical alignment of the system. The testing temperature was maintained by liquid baths whenever possible.

A nitrogen gas cooled crystat which could be controlled to ± 1°C in the temperature range of 0 to -180°C was used for temperatures where a bath was not practical. All temperature measurements were made using a copper-constantan thermocouple with 0°C reference junction. Temperature measurements are estimated to be accurate to within ± 1°C. The final dimensions of the tensile specimens were measured with an optical micrometer, which has a resolution of better than 0.002 mm. However, because the corners of the specimens were rounded due to electropolishing the accuracy of the measured cross-sectional area is estimated to be 3%. This represents the largest error in the data required for stress measurements. All strain measurements were based on crosshead velocity. Only plastic strains are reported in this thesis.

D. Metallography

Optical metallography of transformed single crystals was performed using a Carl Zeiss Ultraphot Photomicroscope II, employing Nemarski interference phase contrast equipment. The Hitachi HU-125 electron microscope was used for all electron microscopy reported in this thesis.

E. Identification of the Martensite Variants of the Orientation Relationship

If single crystals of martensite form in a single crystal matrix of austenite, the variants of the orientation relation which form can be located and identified by using pole figure techniques. A pole figure goniometer is mounted on a x-ray diffractometer (see Fig. 2 and Ref. 13 and 14). The angular rotations about axis A and B of the goniometer, allow the experimenter to scan the total volume of the crystal quickly, looking for the distribution of any pole {hkℓ} simply

by setting the diffractometer angle (axis C) to the appropriate 2θ value, as calculated from Bragg's Law. For this study the distributions of $\{002\}_b$ and $\{10\bar{1}1\}_h$ poles were measured. They were selected because of their high symmetry and the fact that these poles can be scanned without the problem of overlapping reflections. Fekα radiation was used for these measurements.

For the two alloys studied, the orientation relationship between the γ and α phase was found to be the K-S and was confirmed by electron diffraction and x-ray diffraction methods. This result has also been obtained for similar alloys studied.[15-19] Thus close-packed planes and close-packed directions are parallel (within 1-2 degrees) for the γ and α crystals. Alloy 2 contains ε martensite, again existing with close packed γ and ε planes and directions parallel. Because of crystallographic symmetry of the γ-ε interface, specific variants on each {111} plane cannot be resolved by x-ray methods. In other words, the γ-ε interface is also the habit plane for ε martensite. Therefore it is not possible to distinguish between the $(111)_f||(0001)_h$; $[\bar{1}01]_f||[\bar{1}010]_h$, $[\bar{1}10]_f||[\bar{1}100]_h$, and $[0\bar{1}1]_f||[01\bar{1}0]_h$, which are clearly three different variants, one of which would be favored depending on the direction of maximum shear. There is no difficulty in showing that for alloy 2, ε martensite forms on the $\{111\}_f$ plane of maximum shear, provided plastic deformation has occured in the austenite. It is also possible to measure the volume fraction of ε martensite associated with each of the four $\{111\}_f$ planes in the crystal. The 24 variants of the α martensite in the γ martix can all be resolved by the x-ray pole figure method.

With the experimental parameters defined, it was then possible to construct idealized pole figures showing the distribution of $\{002\}_b$ and $\{10\bar{1}1\}_h$ martensite poles in the single crystal austenite matrix. With these poles plotted on a $(111)_f$ sterographic projection, all K-S variants can be resolved and the four resolvable γ-ε variants can be identified. It was assumed that the martensite forms as single crystals in the austenite matrix. The resulting idealized distributions of $\{002\}_b$ poles for the 24 variants of the K-S relationship are plotted in Fig. 3 for a $(111)_f$ orientation. The four orientations of the $\{10\bar{1}1\}_h$ poles are plotted in Fig. 4, again for a $(111)_f$ orientation. The identification of the symbols and numbers on these figures are given in Table II. In order to identify a particular variant, the experimental observations are superimposed onto Fig. 3 or 4. The correlation between the experimental and calculated data was very good and will be discussed in detail later.

F. Volume Fraction Measurements of Each K-S Variant

The approximate position of the $\{002\}_b$ and the $\{10\bar{1}1\}_h$ poles are now known from the automatic pole figure scan of the crystal. The procedure is to relocate each pole manually to the position of the maximum intensity of the peak. The area under the peak was measured by counting the number of x-ray photons of the energy of Fe-kα radiation as the crystal was rotated about axis A (Fig. 2) of the goniometer. These intensities were then corrected for background and compared to the integrated intensity of the $\{002\}_f$ poles. One $\{002\}_b$ pole for each of the 24 K-S variants is found in the circular distribution around one of the three $\{002\}_f$ poles (Fig. 3). All reported quantitative measurements were made in the region surrounding the

three $\{002\}_f$ poles, thus reducing the possibilities of errors due to the angular position of the x-ray beam with respect to the specimen surface. It should be pointed out that the selection of Fekα radiation was made to reduce fluorescent radiation, but more importantly to reduce the variation of intensity as a function of rotations of the specimen in the Schulz pole figure goniometer. Because of geometrical considerations, the larger the 2θ angle of the diffractometer, the larger the angular rotation about axis B (Fig. 2), before intensity errors arise. It has been shown experimentally, using a random polycrystalline quartz sample that if 2θ is greater than 60 degrees, a flat specimen can be rotated about axis B, 70 degrees or more before errors in the observed intensity of the diffracted beam are detected.[13] Using Fekα, 2θ for the $\{002\}_b$, $\{002\}_f$ and $\{10\bar{1}1\}_h$ are 85, 65 and 60 degrees respectively, thus insuring that no errors are present in the intensity measurements for specific poles up to 70° of B axis rotation from the $(111)_f$ pole of the crystal.

Whenever possible intensity measurements were made on a second pole for a particular martensite variant. A second $\{002\}_b$ pole for each of the 24 variants of the K-S orientation relation is present in one of the three rectangular clusters of poles seen in Fig. 3. When adjacent variants were present in this region, the peaks for the two $\{002\}_b$ poles tend to overlap. In all cases where a second pole for a particular variant was independently observable, the intergrated intensity was recorded. The majority of examples where two poles were resolvable, agreement varied between 1 to 5%. For several pole pairs measured, differences as large as 20% were observed. However, the larger differences in integrated intensities were associated with the low volume fraction variants, and the overall error of the

measurement is conservatively 10%. The measurements of volume fraction of two or three phase systems in this manner is described by Cullity.[20] An example of the procedure used to calculate the volume fraction of each variant observed is given in Appendix A.

III. EXPERIMENTAL RESULTS

A. Mechanical Properties and Microstructure

The tensile specimens (Fig. 1) for easy glide ($[\bar{2}\bar{1}3]$ tensile axis) and duplex slip ($[\bar{1}\bar{1}2]$ tensile axis) were obtained from two adjacent elliptical sheets cut from the large crystal for each alloy. The stress-strain data reported in this thesis are plotted as normal stress vs. plastic strain for the duplex slip samples and as resolved shear stress vs. resolved shear strain for the single slip samples. The computer program used to reduce the mechanical property data and plot, using the Cal Comp plotter, is given in Appendix B.

1. Fe-34.5 w/o Ni Alloy

The resulting stress strain curves for the duplex and single slip tensile specimens are given in Figs. 5 and 6 respectively. The initial and final orientation of each specimen is shown in Table III. The specimens tested at 273° and 178°K did not transform to martensite. This observation was confirmed by both optical and x-ray studies, and indicate the M_d temperature for this strain (~5% tensile strain) is at a lower temperature. The slip line structure for the single slip specimen tested at 273°K is shown in Fig. 7. The specimen tested at 177°K has identical appearance. Although the stress strain curve for the single slip specimen shows no sign of work hardening, slip on a second system has taken place as seen in Fig. 7. The magnitude of the step on the crystal for the second slip system is over-emphasized in this micrograph, in that these slip lines disappear as the microscope stage is rotated (Namaski interference contrast equipment used for the majority of metallography presented in the paper), whereas the primary

slip system was always visible to some degree. The micrograph is a compromise in terms of contrast of the two slip systems. It is difficult to say when slip on the secondary system took place, but because of the wavy nature of the slip lines, it is probable that at the start of the tensile test, this slip was required to obtain axial alignment in the Instron testing machine.

The two specimens tested at 121°K transformed to 10% by volume martensite at a tensile strain of 0.050 (duplex slip specimen) and 0.044 (single slip specimen). The duplex slip specimen tested at 121°K was unloaded at 0.03 tensile strain (Fig. 6) to observe why the remarkable increase in hardening rate was occurring. It is clear that duplex slip is nucleating martensite variants, which are obstructing plastic flow of the austenite to a greater extent than was observed for the single slip specimen at the same temperature. An example of the martensite microstructure for the duplex slip specimen is shown in Fig. 8.

The specimens tested at 77°K began to transform in the elastic region of the stress strain curve. The apparent reduction in the flow stress observed is due to the fact that the testing speed is insufficient to offset the volume increase of the crystal due to the $\gamma \rightarrow \alpha$ transformation. These specimens were not used in the quantitative volume fraction measurements. The duplex slip specimen was sectioned and a two surface analysis performed to obtain information on the martensite habit. The relevance of this type of analysis for stress induced martensite is questioned due to the austenite - martensite rotation as a function of plastic strain, and the question of the uniformity of the final austenite orientation. The crystal was

polished on the two perpendicular surfaces, lightly etched, and then each face orientation determined by Laue back reflection. Laue back reflection photos at 5 cm were used to obtain an accurate normal ($\pm 0.5°$) to the crystal surfaces. The results for the two surface normals are [0.5775, 0.5983, 0.5554] and [-0.3703, -0.3809, 0.8472]. The orientation of four martensite plates which intersected the two surfaces were obtained in the conventional manner for this analysis, and the data treated by a simple computer program to obtain the habit plane normal. These results are tabulated in Table IV. An example showing how the measurements were made is given in Fig. 9, and a sample calculation with computer program is given in Appendix C.

2. Fe - 15 w/o Ni - 15 w/o Cr Alloy

The stress strain data for duplex and single slip tensile specimens are given in Figs. 10 and 11 respectively. The initial and final orientation of the crystals are shown in Table III. The specimens tested at 273°K did not transform to martensite in the bulk, however surface martensite which appeared to be associated with intersecting slip traces was observed on the duplex slip specimen. This structure which is shown in Fig. 12 was removed when the specimen was electropolished and etched.

The specimens tested at 242°K were unloaded and removed from the testing machine to see if α martensite was present. None was observed optically, and this was confirmed by x-ray measurements. Both single and duplex slip specimens contained the ε phase in the slip plane(s). The ε is preferentially etched using a FeCl solution. An example showing the ε plates is given in Fig. 13. This etch[21] tends to decorate dislocations causing the pitted surface and reappearance of slip lines in the micrograph.

The specimens tested in the region of 185°K transformed to a characteristic lath martensite, containing both the ε and α phases. The formation of the α phase causes a large reduction in the flow stress at this strain rate. Typical examples of the microstructure of the as crystals are given in Fig. 14. These specimens were electropolished tested crystals are given in Fig. 14. These specimens were electropolished characteristic of the surface, or was related to bulk martensite in the crystal. An example of before polishing, after polishing, and etching the crystal surface is shown in Fig. 15 A, B and C respectively. It is clearly shown that the martensite seen on the as tested surface is related to the bulk crystal.

B. Experimentally Observed Variants of the Orientation Relationship

1. Fe - 34.5 w/o Ni Alloy

The final orientation of the austenite crystals, and the experimental location of the $\{002\}_b$ martensite poles are presented for the single and duplex slip tensile specimens in Figs. 16 and 17 respectively. The arrows represent the tensile axis of the crystal at the end of the tensile test. These specimens were tested at 121°K. The quantitative volume fraction measurements are given in Table V. The two specimens were strained to 5% tensile strain, producing the same volume fraction of martensite ($C_\alpha \approx 0.10$) independent of the number of operating slip systems. The primary difference between the single and duplex slip samples are: the addition of three variants to those observed for single slip and a different distribution of the martensite in the observed variants.

The operating slip plane and direction for the single slip specimen was $(\bar{1}11)_f[0\bar{1}1]_f$, with a Schmid factor of 0.461, and the tensile axis within one degree of the $[\bar{2}\bar{1}3]_f$. The duplex slip specimen was oriented for slip on the $(\bar{1}11)_f[0\bar{1}1]_f$ and $(1\bar{1}1)_f[\bar{1}01]_f$ systems with equal Schmid factors of 0.407. A surprising result was the K-S variant of the orientation relationship with the largest volume fraction of martensite for both crystals is $(111)_f||(110)_b$; $[0\bar{1}1]_f||[\bar{1}1\bar{1}]_b$ (see Table V and Figs. 16 and 17 for details). The K-S variant is associated with the $(111)_f$ plane, the plane of zero shear stress in the austenite crystal. The midrib for the majority of the martensite formed is almost parallel to the tensile axis as is seen in Fig. 9. Thus the shear stresses on the habit planes are also near zero. It is clear the shear direction in the martensite is not in or near the habit plane in this alloy. The direction of shear will of course not be zero in the martensite and must be associated with the maximum critical resolved shear stress on the possible slip or twinning planes in the martensite crystal. Detailed electron microscopy is in progress which will aid in identifying the martensite twinning or slip plane as a function of the austenite orientation.

2. <u>Fe - 15 w/o Ni - 15 w/o Cr Alloy</u>

The final austenite orientation and the experimentally observed $\{002\}_b$ and $\{10\bar{1}1\}_h$ poles for the single and duplex tensile axis crystals are given in Figs. 18 and 19 respectively. The single and duplex crystals were tested at 188°K and 181°K respectively. Although both ε and α martensite were formed, the variants formed were those associated with the slip plane. The single and duplex slip crystals were strained to 5% tensile strain, producing a total $(C_\alpha + C_\varepsilon)$ volume

fraction of 0.089 and 0.058 martensite respectively. The distribution of α and ε martensite for these crystals are given in Table VI.

The slip system for the single slip specimen was $(\bar{1}11)_f[0\bar{1}1]_f$ with a Schmid factor of 0.455. The variant of the orientation relationship with the largest volume fraction of α martensite is the $(\bar{1}11)_f||(110)_b$; $[0\bar{1}1]_f||[\bar{1}1\bar{1}]_b$, showing a strong dependence between the slip direction and the martensite variant formed. The duplex slip specimen was not perfectly orientated with the $(1\bar{1}1)_f[\bar{1}01]_f$ slip system having a Schmid factor of 0.417 and the $(\bar{1}11)_f[0\bar{1}1]_f$ slip system having a Schmid factor of 0.366. This orientation caused the $(1\bar{1}1)_f||(110)_b$; $[\bar{1}01]_f||[\bar{1}11]_b$ K-S variant to contain the majority of the α martensite. However, martensite was formed due to both slip systems as is shown in Table VI. The ε martensite formed in both crystals was related to the slip plane, i.e. $\{111\}_f||\{0001\}_h$. A result which is not understood for the moment is the observed presence of $\{10\bar{1}1\}_f$ poles parallel to the $\{111\}_f$ poles which are seen in Figs. 18 and 19. The first thoughts were these poles were due to twinning of the ε phase. However, this apparently is not the case, at least for the common twinning system in hcp materials. Diffractometer scans over 2θ were made between the $\{111\}_f$ to the $\{10\bar{1}1\}_h$. This produced two resolvable peaks. However the $\{111\}_f$ peaks were very broad, and appeared to overlap to some degree in the region of the $\{10\bar{1}1\}_h$ 2θ value. Thus it is possible that the intensity measured was due to the overlap of the very broad $\{111\}_f$ peak. The other explanation is that a second orientation relationship exists for ε martensite. The experiment to resolve this problem would be to examine a thin foil cut so the plane of the foil is $\{111\}_f$; then look for the presence of the hcp phase with $\{111\}_f||\{10\bar{1}1\}_h$. This experiment has not been done.

IV. DISCUSSION

A. Plastic Flow in Face Centered Cubic Austenite

The temperature dependence of the flow stress in face centered cubic crystals is generally low, thus plastic flow is primarily due to long range stress fields and the short range obstacles (Peierls force) can be overcome for the most part by thermal activation alone. In the case of ferromagnetic austenites, however, a very strong temperature dependence of the flow stress is observed, requiring a much larger thermal component of the stress for glide, indicating a different dislocation mechanism for glide in these face centered cubic crystals. Also observed experimentally is a reversal of the flow stress at the onset of the γ-α martensite transformation (Fig. 20), which was explained away in terms of geometrical factors and testing conditions. However, this may not be true. Finally the morphology of the martensite of the low stacking fault alloy is lath-like and that of high stacking fault ferromagnetic Fe-Ni alloy is plate-like (Fig. 8). In addition to the remarkable difference in the appearance of the martensite, an equally remarkable difference in the distribution of the martensite variants is observed. These results will be presented in detail in the next section. For now it is interesting to note that in single crystals tested in tension, the variants of the orientation relation observed experimentally for alloy 2 (lath-type martensite) are all related to the slip plane, with the slip vector being associated with the variant of maximum volume fraction of martensite. Alloy 1 on the other hand produced martensite related to the austenite (111) plane of zero shear stress, but was also associated with the slip vector in the crystal. Clearly plastic flow in these crystals which give rise

to the formation of the martensite embryo is different in these two alloys. It appears that both the role of stacking fault energy in paramagnetic Fe-Ni-Cr alloys and the effect of ferromagnetism in Fe-$\langle$28% Ni alloys, must be considered in terms of their role in modifying the deformation characteristics in these crystals, if any insight into the dislocation interaction required for the nucleation of the martensite phase in these alloys is to evolve.

There is indirect evidence that the stacking fault energy may be a key factor in the nucleation of martensite, at least for alloys containing the hexagonal close packed phase. Cobalt for example undergoes a martensite transformation. Here the transformation is f.c.c. to h.c.p. The h.c.p. structure suggests the possibility of this transfromation beginning from a single stacking fault. The transformation may be accomplished if a shockley partial dislocation of Burgers vector $a/6\langle 11\bar{2}\rangle$ moves through alternate atomic planes of a parallel set of {111} planes.[22] In low stacking fault energy stainless steel alloys, when ε martensite is present, the martensitic transformation observed is $\gamma \rightarrow \varepsilon \rightarrow \alpha$. The ε phase was first identified by Venables,[23] producing a good deal of discussion about its importance. The primary question was, does the ε martensite form before or after the α phase? This has been resolved in 304 stainless steel by Mangonon and Thomas,[24] who showed that the transformation is $\gamma \rightarrow \varepsilon \rightarrow \alpha$. In the present work, ε martensite has been shown to exist in the absence of α for alloy 2, a result which is predicted thermodynamically by Breedis and Kaufman.[25] The ε phase is not observed experimentally in high stacking fault energy iron alloys.

In low stacking fault alloys, the presence of ε is not a requirement for the γ → α transformation. Goodchild et al.,[11] have shown that 301 and 305 stainless steel grains subjected to tension along the ⟨001⟩ axis contain no ε or stacking faults. The α which is formed in grains with a tensile axis near ⟨001⟩ is thus not in association with ε martensite. In the present single crystal study, α forms with specific K-S variants associated to the slip plane, with ε always present (alloy 2). What Goodchild's results suggest is, in low stacking fault alloys, two specific types of α nucleation are taking place, one type associated with the faulted crystal and the other associated with a network of dislocations in the absence of faults. Therefore in the same alloy, one can observe the transformation proceeding as γ → ε → α or γ → α, the presence of ε being simply a function of crystal orientation. When ε is present the transformation is always ε → α. For crystals orientated to favor the formation of ε martensite, it is not supprising to have observed all α martensite formed to be in association with the K-S variant related to the operating austenite slip plane. This is because the ε martensite must be in the slip plane due to the mechanism by which it forms. It is possible K-S variants for the α martensite may be observed which are not in the slip plane for alloy 2, if a crystal can be orientated to suppress the ε martenstie formation. This appears to be the case in Goodchild's alloys when observations were made on grains stressed in tension along the ⟨001⟩ axis. An interesting experiment would be to pull a single crystal of alloy 2 with a ⟨001⟩ tensile axis and observe if α martensite formed on the 4 equally favored slip systems, does in fact form with a total absence of ε martensite. If this

experiment is successful, nucleation of deformation induced martensite may be studied which is associated with dislocation networks and or the faulted crystal in the same single crystal alloy.

The width of a dissociated dislocation as a function of dislocation velocity (applied stress) has been studied by Copley and Kear[26]. They have developed a model which places, on a quantative basis, the separations of the leading and following Shockley partial dislocations as a function of the critical resolved shear stress on each dislocation. The relationship expressed in terms of the Schmid factors is,

$$\frac{1}{\Delta X} = \frac{1}{C}\left(\gamma \pm \frac{(m_2-m_1)}{2}\sigma b\right) \qquad (1)$$

where ΔX is the distance between the partial dislocations, γ is the stacking fault energy, m_1 and m_2 are the Schmid factors for the Shockley partials, σ is the normal stress and b is the Burgers vector. The constant C is a material parameter which is written as,

$$C = \frac{\mu a^2}{48\pi(1-\nu)}\left[2 - \nu(4\cos^2\phi - 1)\right] \qquad (2)$$

where μ is the shear modulus, a is the lattice parameter and ϕ is the angle between the dislocation line and the resultant Burgers vector of the Shockley pair. A tensile specimen with the tensile axies within the portion of the unit triangle bounded by the [001], [113] and [102] will have a larger shear stress on the moving, trailing Shockley partial dislocation, thus reducing the equilibrium separation. The leading Shockley partial dislocation has the greatest resolved shear stress in the regions bounded by the [111], [101], [102] and [113]

of the unit triangle. The great circle connecting the [113] and [102] has equal Schmid factors for each of the Shockley partial pairs. The situation is reversed for compression in these regions. The separation, ΔX, has been calculated as a function of dislocation velocity[26] using the Gilman equation for dislocation velocity as a function of stress.

$$V = v^{*} \exp\left(-\frac{D}{\tau}\right) \qquad (3)$$

v^{*} is approximately equal to the shear wave velocity of the material and D is the frictional drag acting on the moving dislocation, having the dimension of stress. As the dislocation velocity approaches v^{*}, the separation of the partials approaches zero for a ⟨ 001 ⟩ tensile axis and large values for tensile specimens on the [111] to [101] great circle. An example of this calculation is given in Fig. 21. A quantative correlation of the role dissociated dislocations have as a function of dislocation velocity (stress) on the formation of ε martensite is now possible; an experiment which has not been done. It also appears that M_d for α martensite may be lowered for orientations where the separations of partials approach zero, i.e., the ⟨ 001 ⟩ tensile axis. When ε is present, α martensite is always associated with the most active slip plane for orientations studied in this paper. The experiment mentioned, that of pulling a ⟨ 001 ⟩ specimen of alloy 2, may show martensite variants not associated with the active slip plane, as was observed for the high stacking fault energy alloy 1. If this is so, then dislocation networks are responsible for nucleation in alloy 1, and the effect is not due to some magnetic property of the ferromagnetic austenite.

In ferromagnetic Fe-Ni alloys the strong temperature dependence of the flow stress appears to be related to the Curie temperature of the alloy. Nabarro[28] points out that plastic flow will lead to changes in the magnetostriction which could produce or relax internal stresses in different directions than that of the applied external stress. It is possible that this anisotropy due to magnetostriction could cause a change in the Burgers vector of the glide dislocations. Bolling and Richman[29] feel the strong temperature dependence of the flow stress in Fe-Ni alloys is due to the ferromagnetism of these alloys, implying again a change in mechanism or configuration of the glide dislocation in ferromagnetic alloys. Seeger et al.[30] have shown that domain wall mobility is decreased by the presence of dislocations (plastic deformation) which could cause internal stress due to magnetostriction, important in terms of nucleation of the martensite.

Alloy 1 is of the Invar type and has a negative coefficient of thermal expansion to the Curie temperature. Above the Curie temperature, these alloys behave in the normal manner with a positive coefficient of thermal expansion. The magnetostriction forces are large enough to overcome the increase in thermal energy in the crystal. It is possible that the applications of the applied stress on these crystals causes a magnetic dilatation over and above the Poisson effect, thus generating large anisotropic stresses not associated with the external stress, but as a consequence of the external stress. This could be the reason different α martensite variants are observed forming in alloy 1, than where observed for alloy 2.

It is not possible at the present time to define the role that ferromagnetism may play in dislocation motion and configuration, in

terms of the martensite embryo. If ferromagnetism is not important in the nucleation process, then it is possible studies should be concentrated on the relationship between specific dislocation configurations (faulted and dislocation networks in the austenite) and the specific martensite variants which are observed to form.

B. Effect of Crystal Orientation on the Martensite Transformation

1. Fe-34 w/o Ni Alloy

The single slip specimen ($[\bar{2}\bar{1}3]$ tensile axis) tested at 121°K to 5% tensile strain, transformed to 10.7 volume percent α martensite; 8 volume percent was the $(111)_f||(110)_b$; $[01\bar{1}]_f||[\bar{1}1\bar{1}]_b$ K-S variant. For this K-S variant, foils prepared for transmission electron microscopy with a $(\bar{1}\bar{1}2)_f$ orientation should have an abundance of martensite plates of the $(1\bar{1}3)_b$ orientation. This result was observed, examples of which are given in Figs. 22a and b. Both dislocated (Fig. 22a) and twinned (Fig. 22b) α martensite were observed. An insufficient number of foils was observed to obtain a feeling for the ratio of twinned to dislocated martensite, except to say that fully twinned martensite plates should be the dominant structure in this alloy. These observations are confirmed by comparing the orientations of the dislocated and twinned plates in Fig. 22 to those on the $(\bar{1}\bar{1}2)_f$ surface of Fig. 9. The trace of the partially twinned-dislocate martensite crystal in Fig. 22a makes an angle of 39.3° to the $[111]_f$ direction. Plates of this orientation are rare on the $(\bar{1}\bar{1}2)_f$ surface of Fig. 9, and tend to be split off from a large plate of slightly different orientation. The trace of the fully twinned martensite crystal in Fig. 22 makes an angle of 48° with the $[111]_f$ direction, an angle observed frequently on the $(\bar{1}\bar{1}2)_f$ surface of Fig. 9.

It is clear from these observations that the habit plane in this alloy will depend on the mode of accomodation deformation. Because the habit planes for dislocated, dislocated-twinned, and fully twinned martensite can vary in the same alloy, as shown above, habit plane measurements without detailed metallography are of little use. Also habit plane measurements for comparison with the classical theory are of little use because the theories cannot account for the varied accomodation deformation observed in neighboring regions of the same specimen.

The habit plane measurements made by two surface analysis in this study are given in Table IV. The results show the measured habits were within 4-10° of the classical $(3\ 10\ 15)_f$ habit. It has been possible to use these measurements to obtain the specific habit plane normal from a single trace on an electron micrograph. The specific K-S variant is obtainable from the overlapping electron diffraction patterns. It is therefore possible to obtain both the K-S variant and habit plane normal from an electron micrograph and appropriate electron diffraction patterns. When a single trace of a twinned martensite plate from a $(\bar{1}\bar{1}2)_f$ foil is compared to the 24 possible variations of the mean habit observed (Table IV), only one possible solution has been observed. The trace of the partially twinned plate in 22a does not lie in any of the 24 possible habits; i.e., the dot produce for no case is 90° from the habit plane normal measured experimentally. The trace of fully twinned plates in Fig 22 are within 89-91 degrees of a specific habit plane normal, and thus within experimental error, the specific habit plane is identified. This technique will be used in the continuing study of this alloy. The electron microscope

provided detailed microstructural information about the martensite crystal. If the electron microscope images of specific microstructures can be correlated to the optical images so that accurate habit plane normals can be calculated, a more detailed understanding as to why large variations exist in experimentally measured habit planes will evolve.

The observed habit planes of the deformation induced martensite plates with respect to the tensile axis in this alloy was not expected. The majority of the martensite plates formed, in each specimen tested, has the plane of the plate almost parallel to the tensile axis as seen in Figs. 8 and 9. The martensite-martensite interfaces noted as 6 and 5 in Fig. 9c have plane normals of [-0.7315, 0.6692, -0.1306] and $[-0.7032, 0.6909, 0.1680]_f$ respectively. These are near the habit planes for individual plates seen in Fig. 9a. It is easy to see the shear stress on these habits is low and it has been pointed out by the x-ray data that the K-S variant of zero shear in the austenite is the variant 80% of the martensite formed in this alloy. The stress induced transformation in this alloy is not following the relationship developed by Patel and Cohen,[4] where it is shown the martensite variant which should form, is the variant of maximum shear stress on the habit plane. The work of Goodchild et al.[5] on 303 and 305 stainless steels supports the concepts of Patel and Cohen,[4] which makes one again think of some sort of magnetic effect which is modifying the internal stresses in these ferromagnetic crystals.

2. <u>Fe-15 w/o Ni-15 w/o Cr Alloy</u>

The martensite induced due to plastic deformation in these crystals form on K-S variants related to the active slip planes in the

crystals. The ε martensite is shown to form as a strong function of crystal orientation. The duplex slip specimen was not in a perfect duplex orientation causing a two-fold increase in the volume fraction of ε in the most active slip plane. The volume fraction of α on the most active slip plane was an order of magnitude larger than that observed on the second slip plane in the crystal. The nucleation of α martensite is therefore closely associated to the movement of dislocations in the slip plane and the initial formation of ε in this alloy. In alloy 1 the volume fraction of α was almost equal for equal tensile strain for both the single and duplex specimens. In alloy 2, the $[\bar{1}\bar{1}2]_f$ tensile specimen contained only 5.8% $(C_\alpha + C_\varepsilon)$ martensite as compared to 8.9% $(C_\alpha + C_\varepsilon)$ martensite for the $[\bar{2}\bar{1}3]_f$ tensile sample. The quantity of α martensite formed in the duplex slip specimen was suppressed; only 2.9% α martensite as 6.8% for the single slip specimen was observed. It is again clear that the formation of ε martensite is a strong function of crystal orientation, which in turn controls by aiding or abeting the $\varepsilon \rightarrow \alpha$ transformations. For the orientations tested to date, it is not completely clear why the transforamtions should be different in terms of the relative amounts of α observed for the $[\bar{1}\bar{1}2]_f$ and $[\bar{2}\bar{1}3]_f$ tensile axis samples which were tested to the same tensile strain. The results of Goodchild, et al.[5] show that ε is suppressed for crystals with a $\langle 001 \rangle_f$ tensile axis and the M_d for α is lowered for these orientations.

Experiments are in progress where specimens with $[110]_f$ and $[001]_f$ tensile axes orientations will be tested and volume fraction measurements made of the ε and α martensite variants formed. These data will shown that the resolved shear stress on the leading and trailing

partials will control the dynamic separations of moving partial dislocations, and thus will strongly control the nucleation of ε martensite. It appears clear at this time that for low stacking fault energy alloys, where ε can form, the M_d for α is higher in the presence of ε. If for ⟨001⟩ tensile axis crystals, ε martensite is absent, it will be interesting to observe if the α forms with the same blocky microstructure, or if in fact the martensite is of the massive type.

The temperature M_d for ε and α martensite is of considerable interest because of the role it plays in defining heat treating and deformation parameters. From a scientific point of view one would like to know if M_d can be described in thermodynamic terms. Patel and Cohen[4] have shown for stress induced martensite (stress less than the proportional limit) the experimentally observed M_d for α can be calculated with good accuracy by considering the work done by the external force. So in the temperature range where the stress induced transformation is observed, the M_d appears to be a thermodynamic function. When the temperature is raised it is still possible to induce the transformation by plastic deformation of the crystal. For the strain induced transformation the M_d is now a function of the external force, the temperature and the degree of plastic deformation. As the temperature is increased the transformation will start at increasing plastic strain levels. For single crystals orientated for easy glide very little increase in stress is observed with increasing strain. For these crystals the transformation starts at a specific plastic strain level which is a strong function of temperature and only a minor function of stress. This behavior is very difficult to describe thermodynamically. A second problem which complicates the

matter is the presence of ε martensite as is the case for alloy 2. Very little is known about the M_d for ε martensite. Plastic deformation of the austenite is required for the $\gamma \rightarrow \varepsilon$ transformation. When ε martensite is present the reaction is $\gamma \rightarrow \varepsilon \rightarrow \alpha$, in this case the observed M_d for α is at a higher temperature than for the $\gamma \rightarrow \alpha$ reaction. In polycrystalline samples α martensite would be nucleating at two different temperatures, depending on the crystal orientations of the austenite grains and the direction of the applied stress. As work on these single crystal alloys continues much of the effort will be directed toward a detailed studied of M_d for both ε and α martensite as a function of stress, strain and temperature. Efforts will be made to describe the experimentally observered characteristics of M_d for strain induced martensite thermodynamically.

V. SUMMARY AND CONCLUSIONS

Single crystals have been used to study the martensite transformation in Fe-Ni and Fe-Ni-Cr alloys. It has been shown the transformation in these alloys is a strong function of crystal orientation. For alloy 1, it was found the deformation induced martensite favored a specific K-S variant which was associated with the $\{111\}_f$ plane of zero shear stress in the austenite. The habit planes observed in alloy 1 for martensite plates formed during plastic deformation, for the most part were planes almost parallel to the tensile direction; thus the shear stress on the habit plane is also near zero. It is clear the direction of the shear in the martensite plates cannot be zero, the direction of which is yet to be determined by experiment. The fact that 80% of the martensite observed in alloy 1 was associated with the austenite plane of zero shear invited speculation that a magnetic dilatation due to magnetostrictive forces may be modifying the internal stresses of the crystal which are a consequence of the externally applied stress in these ferromagnetic austenites. This is mere speculation at this time, and it is more likely the transformation proceeds in this manner due to the absence of the ε phase, which is observed in alloy 2.

In alloy 2 the transformation reaction $\gamma \rightarrow \varepsilon \rightarrow \alpha$ was observed for the crystal orientations studied. The ε martensite was found to form in the operating slip plane(s) in all cases. Because of this property of the reaction, and the fact the reaction continues from ε to α, the majority of α martensite was found to be the K-S variant associated with the slip plane(s) of the crystal. There is evidence that for $\langle 001 \rangle_f$ crystal orientations, the ε martensite phase can be

suppressed.[5] If this is found to be the case for alloy 2 then the $\gamma \rightarrow \alpha$ reaction can be observed independent of the ε phase. This may prove to be very important in terms of understanding the reaction in alloy 1. This is because the same K-S variant may form as a function of the applied stress in alloy 2, in the absence of ε martensite, as was observed in alloy 1. If this result is found, then the idea of a magnetic interaction in alloy 1 can be rejected.

Habit plane measurements on alloy 1 were performed. It was found when accurate habit plane data were available, the habit plane of a crystal could be identified by the single trace observed in electron micrographs. Because the K-S variant is always obtainable if the overlapping electron diffraction pattern of γ and α are obtained, it was possible (for alloy 1) to identify both the martensite habit and K-S variant in electron micrographs. The development of this type of data will aid in relating the state of stress in the crystal to the microstructural details observed in the martensite crystals from electron micrographs, and therefore should aid in developing and understanding some of the basic properties of the transformation. Habit plane measurements for alloy 2 have not been possible by two surface analysis because of the blocky nature of the martensite as seen in the optical micrographs (Fig. 14). The x-ray results of alloy 2 have shown that ε will exist in the absence of α. The quantative volume fraction measurements are in progress for the $[\bar{1}\bar{1}2]$ and $[\bar{2}\bar{1}3]$ tensile axis specimens, and will be combined with the data of the [110] and [001] tensile axis specimens to produce an interesting set of data showing how the volume fraction of ε varies at constant tensile strain and temperature as a function of crystal orientation in the absence of α.

0 0 0 0 3 6 0 0 5 7 2

The primary result of this thesis is the application of pole figure methods to locate and identify the specific K-S variants for α martensite and variants of ε martensite which are formed by deformation in the austenite single crystal. The ability to measure quantatively the volume fraction of each variant provides the important information about the relative amounts of martensite that form as a function of the austenite crystal orientation. It has been discussed many times in the literature that the martensite tends to form in very specific variants as a function of stress. As far as this investigator knows this is the first presentation of a method in which the specific variants can be identified as a function of the state of stress and the volume fraction of each variant measured. This type of information is of critical importance if the martensite nucleation problem is to be approached in a systematic manner.

Although there are many questions left unanswered in this paper, it is felt that the basic knowledge and experimental methods have been developed to answer them with more work and experiment. It is hoped that this thesis will form a sound basis for the continuation of the study of the martensite nucleation problem in these Fe-Ni and Fe-Ni-Cr single crystal alloys and that some fundamental knowledge will develope in the work that is to follow.

ACKNOWLEDGMENTS

The author wishes to thank his ex-wife, Janet for the encouragement and help received during our many years together. Many thanks are due to Jenifer Hunn for her wonderful common sense and friendship; without her help this thesis would have never been completed. I would like to give special thanks to Professor Thomas, not only for his constant encouragement and technical guidance, but for his unending patience during a difficult period. Also many thanks to my colleage Lutgard DeJonge for helpful discussions, to Omer Van Der Biest for helping with the lattice parameter measurements, and to Professors E. R. Parker and R. Wenk for reading the manuscript. The alloys single crystals used in this study were grown by the Advanced Materials Research and Development Laboratory of Pratt and Whitney Aircraft.

This work was performed under the auspices of the United States Atomic Energy Commission.

APPENDIX A

Method of X-ray Volume Fraction Measurements

The procedure used to calculate volume fraction (C_i) of ε and α martensite is that of Cullity.[20] The diffracted intensity for each phase is given by:

$$I_\gamma = \frac{K_2 R_\gamma C_\gamma}{2\mu m} \tag{1}$$

$$I_\alpha = \frac{K_2 R_\alpha C_\alpha}{2\mu m} \tag{2}$$

$$I_\varepsilon = \frac{K_2 R_\varepsilon C_\varepsilon}{2\mu m} \tag{3}$$

where K_2 is a numerical constant which drops out by taking ratios of Eqs. (1) through (3), and

$$R = \left(\frac{1}{v^2}\right)\left[|F|^2 \; P \left(\frac{1 + \mathrm{Cos}^2\theta}{\mathrm{Sin}^2\theta\mathrm{Cos}\theta}\right)\right] (e^{-2m}) \tag{4}$$

where v is the volume of unit cell, F is the structure factor, P is the multiplicity factor, $\left(\frac{1 + \mathrm{Cos}^2\theta}{\mathrm{Sin}^2\theta\mathrm{Cos}\theta}\right)$ is the Lorentz-Polarization factor for unpolarized x-rays, e^{-2m} is the temperature factor which is a function of θ, the Bragg angle and μ_m is the linear absorption coefficient.

Because a single reflection is used to measure the intensity of the γ, α and ε phases, the multiplicity factor is taken as unity. A unique solution for the volume fraction is obtained by using the following relationship in conjunction with Eqs. (1) through (3).

$$C_\gamma + C_\alpha + C_\varepsilon = 1 \tag{5}$$

Thus by taking the ratios I_α/I_γ and I_ε/I_γ and using Eq. (5), there exist three equations and three unknowns, or two equations and two unknowns as the case may be. The R values for each phase of the two alloys are calculated in the conventional manner.[20] The structure factor F has been corrected for anomalous scattering.

The total volume fraction of each phase was obtained by summing the total intergrated intensity of the observed $\{002\}_b$ and $\{10\bar{1}1\}_h$ poles for the α and ε phases respectively and comparing them to the intergrated intensity of the $\{002\}_f$ poles. The volume fraction for each variant was then calculated by the following relationship.

$$C_{i\alpha} = \left(\frac{I_i}{I_\alpha}\right) C_\alpha \tag{6}$$

or

$$C_{i\varepsilon} = \left(\frac{I_i}{I_\varepsilon}\right) C_\varepsilon \tag{7}$$

where I_α and I_ε are the total intergrated intensity of these phases, I_i the intergrated intensity of a particular variant and C_α and C_ε are the total volume fraction of each phase.

APPENDIX B

Computer Program for Mechanical Property Data Reduction and Cal Comp Plotting

The Figs. 5, 6, 10 and 11 were plotted in a one step calculation from the Instron strip chart recording of the load elongation curves for the single crystal tensile specimens. No hand calculations were required and only minor touch up of the Cal Comp plots were needed before they could be photographed for publication. The input data are specimen width, thickness and gauge length. The Instron data needed are crosshead speed, chart speed and Instron load cell setting. From the load elongation curve, the number of chart divisions in the load and elongation axes are punched on data cards for as many data points required. The more data points used the better, because the Cal Comp plotter draws straight lines between data points. The first data point must be the proportional limit. Because the Instron is not a hard machine, this data allows machine and fixture deflections to be corrected for and the resulting calculations are based on plastic strain. The total crystal and machine deflection is measured from the origin.

The SUBROUTINE GRAPH requires no additional input data and is set up in the listing to generate plots of the type seen in Figs. 5 and 10. The program can be modified to produce plots of any scale range required. Any number of stress strain curves may be plotted on a single frame and any number of frames may be plotted at one time.

The data deck is set up as follows:

Card 1: The number of stress strain curves to be plotted on the first frame; I2 format.

Card 2 and 3: Title card; 80A1/80A1 format.

Card 4: Crosshead and chart speed; F7.4, F4.1 format.

Card 5. Gauge length, width and thickness; F8.4, 2F6.4 format.

Card 6: Phi and Lambda where Phi is the angle between the slip plane normal and the tensile axis, and Lambda is the angle between the slip direction and the tensile axis of the crystal. For polycrystal samples set Phi and Lambda equal to 45 degrees. 2F5.1 format.

Card 7: Instron load scale; F6.0 format.

Card 8: Key to units used; I2 format. Set KEY=1 if units are cm/min for crosshead and chart speed, mm for specimen dimensions and Kg for load scale. Set KEY=2 if units are inches/min for crosshead and chart speed, inches for specimen dimensions and lbs for load scale.

Card 9: Six pairs of load-elongation data per card; 12F6.1. Data is in chart divisions, with a division being defined as 1/10 of an inch or 1/5 of a cm. As many of these cards may be used as needed. Indicate end of data set by punching a negative stress after the last real pair of data points. The first data pair must be the proportional limit.

Repeat the data card sequence from Card 2 to 9 the number of times specified on Card 1. These data will be plotted on the same frame. For the next frame and so on, start over from Card 1. To end calculations, the last card of the data deck will be Card 1 with zero punched in Column 2. An example of the correct form for the input data and the resulting output data is given in Table VII. The Fortran listing follows.

```
      PROGRAM CRYSTAL(INPUT,OUTPUT,TAPE6=INPUT,TAPE5=OUTPUT,TAPE98,PLOT,
     1TAPE99=PLOT)
      DIMENSION TITLE1(160),TITLE2(69),TITLE3(60),TITLE4(70),
     1TITLE6(74),TITLE7(78),DATA(12),TABLE(6,200)
    1 FORMAT(I2)
    2 FORMAT(80A1/80A1)
    3 FORMAT(1H1,30X,10HINPUT DATA//)
    4 FORMAT(F7.4,F4.1,69A1)
    5 FORMAT(F8.4,2F6.4,60A1)
    6 FORMAT(2F5.1,70A1)
    8 FORMAT(F6.0,74A1)
    9 FORMAT(I2,78A1)
   10 FORMAT(12F6.1)
   11 FORMAT(5H LOAD,6X,6HCHANGE,4X,6HSTRESS,6X,6HSTRAIN,4X,5HSHEAR,7X,
     15HSHEAR/10X,9HIN LENGTH,24X,6HSTRESS,6X,6HSTRAIN/4H  KG,9X,2HMM,6X
     2,8HKG/MM**2,13X,8HKG/MM**2/)
   12 FORMAT(1H ,F7.2,3X,F7.4,3X,F8.3,3X,F8.5,3X,F8.3,3X,F8.5)
   13 FORMAT(     80A1/80A1//)
   14 FORMAT(//,30X,11HOUTPUT DATA//)
   15 FORMAT(1H1,30X,11HOUTPUT DATA//)
   16 FORMAT(//12HSTRAIN RATE=,F7.5,9H PER MIN.,5X,18HSHEAR STRAIN RATE=
     1,F7.5,9H PER MIN.//)
  110 READ(6,1) NUMBER
      IFIRST=0
      IF(NUMBER.EQ.0) 111,112
  111 CALL GRAPH(TABLE,-1,IFIRST)
      STOP
  112 DO 999 I=1,NUMBER
      READ(6,2) TITLE1
      WRITE(5,3)
      WRITE(5,13) TITLE1
      READ(6,4) CHS,CS,TITLE2
      WRITE(5,4) CHS,CS,TITLE2
      READ(6,5) GAUGE,WIDTH,THICK,TITLE3
      WRITE(5,5) GAUGE,WIDTH,THICK,TITLE3
      AREA=WIDTH*THICK
      READ(6,6) PHI,LAMBDA,TITLE4
      WRITE(5,6) PHI,LAMBDA,TITLE4
      PHI=PHI*3.1416/180.
      LAMBDA=LAMBDA*3.1416/180.
      READ(6,8) SCALE,TITLE6
      WRITE(5,8) SCALE,TITLE6
      READ(6,9) KEY,TITLE7
      WRITE(5,9) KEY,TITLE7
      CROSSH=CHS
      IF(KEY.EQ.1) CROSSH=CHS*10.
      SRATE=CROSSH/GAUGE
      SSRATE=(((GAUGE+CROSSH)/GAUGE)**2-(SIN(LAMBDA)**2))**0.5/SIN(1.570
     18-PHI)-COS(LAMBDA)/SIN(1.5708-PHI)
      L=0
      N=22
      JFIRST=0
  104 READ(6,10) DATA
      N=N+1
      WRITE(5,10) DATA
      IF(KEY.EQ.2) GO TO 100
      DO 101 J=1,12,2
```

```
      IF(DATA(J))103,102,102
  102 K=J+1
      L=L+1
      TABLE(1,L)=DATA(J)*SCALE/100.
      IF(JFIRST) 113,113,114
  113 JFIRST=1
      SLOPE=DATA(K)/TABLE(1,L)
  114 TABLE(2,L)=(DATA(K)-TABLE(1,L)*SLOPE)*(CHS/(CS*5.0))*10.0
      IF(TABLE(2,L).LT.0.0)  TABLE(2,L)=0.0
      TABLE(3,L)=TABLE(1,L)/AREA
      TABLE(4,L)=TABLE(2,L)/GAUGE
      TABLE(5,L)=TABLE(3,L)*COS(PHI)*COS(LAMBDA)
  101 TABLE(6,L)=(((GAUGE+TABLE(2,L))/GAUGE)**2-(SIN(LAMBDA))**2)**0.5/
     1SIN(1.5708-PHI)-COS(LAMBDA)/SIN(1.5708-PHI)
      GO TO 104
  100 DO 105 J=1,12,2
      IF(DATA(J))103,106,106
  106 K=J+1
      L=L+1
      TABLE(1,L)=DATA(J)*SCALE/100.0*0.453592
      IF(JFIRST) 115,115,116
  115 JFIRST=1
      SLOPE=(DATA(K)/TABLE(1,L))*0.453592
  116 TABLE(2,L)=((DATA(K)-TABLE(1,L)*SLOPE/0.453592)*CHS/(CS*10.0))*25.
     14
      IF(TABLE(2,L).LT.0.0) TABLE(2,L)=0.0
      TABLE(3,L)=TABLE(1,L)/(AREA*25.4*25.4)
      TABLE(4,L)=TABLE(2,L)/(GAUGE*25.4)
      TABLE(5,L)=TABLE(3,L)*COS(PHI)*COS(LAMBDA)
  105 TABLE(6,L)=(((GAUGE*25.4+TABLE(2,L))/(GAUGE*25.4))**2-(SIN(LAMBDA)
     1)**2)**0.5/SIN(1.5708-PHI)-COS(LAMBDA)/SIN(1.5708-PHI)
      GO TO 104
  103 WRITE(5,14)
      WRITE(5,16) SRATE,SSRATE
      WRITE(5,11)
      DO 107 IA=1,L
      N=N+1
      IF(N.EQ.61) GO TO 108
  109 WRITE(5,12) (TABLE(JA,IA),JA=1,6)
      GO TO 107
  108 WRITE(5,15)
      WRITE(5,13) TITLE1
      WRITE(5,11)
      N=9
      GO TO 109
  107 CONTINUE
      CALL GRAPH(TABLE,L,IFIRST)
  999 CONTINUE
      GO TO 110
      END
      SUBROUTINE GRAPH(TABLE,L,IFIRST)
      DIMENSION TABLE(6,200),X(200),Y(200),GRIDX(2),GRIDY(2)
      COMMON/CCPOOL/XMIN,XMAX,YMIN,YMAX,CCXMIN,CCXMAX,CCYMIN,CCYMAX
      DATA XMIN,XMAX,YMIN,YMAX/0.0,0.125,16.0,64.0/
      CCYMIN=100.
      CCYMAX=1000.
      IF(L) 100,100,101
```

```
100 CALL CCEND
    RETURN
101 IF(IFIRST) 102,102,103
102 IFIRST=1
    CALL CCNEXT
    CALL CCGRID(1,6HNOLBLS,1)
    GRIDY(1)=16.0
    GRIDY(2)=17.0
    DO 108 I=1,12
    GRIDX(1)=I*0.01
    GRIDX(2)=GRIDX(1)
    CALL CCPLOT(GRIDX,GRIDY,2,4HJOIN)
108 CONTINUE
    GRIDX(1)=0.1225
    GRIDX(2)=0.125
    DO 109 I=18,62,2
    GRIDY(1)=I
    GRIDY(2)=I
    CALL CCPLOT(GRIDX,GRIDY,2,4HJOIN)
109 CONTINUE
    GRIDY(1)=64.
    GRIDY(2)=63.
    DO 110 I=1,12
    GRIDX(1)=I*0.01
    GRIDX(2)=GRIDX(1)
    CALL CCPLOT(GRIDX,GRIDY,2,4HJOIN)
110 CONTINUE
    GRIDX(1)=0.0
    GRIDX(2)=0.0025
    DO 111 I=18,62,2
    GRIDY(1)=I
    GRIDY(2)=I
    CALL CCPLOT(GRIDX,GRIDY,2,4HJOIN)
111 CONTINUE
    CALL CCLTR(300.,40.,0,3,21H        PLASTIC STRAIN,21)
    CALL CCLTR(20.,250.,1,3,28H         NORMAL STRESS, KG/MM,28)
    CALL CCLTR(10.,839.,1,2,1H2,1)
    CALL CCLTR(65.,80.,0,2,1H0,1)
    CALL CCLTR(130.,80.,0,2,3H.01,3)
    CALL CCLTR(210.,80.,0,2,3H.02,3)
    CALL CCLTR(290.,80.,0,2,3H.03,3)
    CALL CCLTR(370.,80.,0,2,3H.04,3)
    CALL CCLTR(450.,80.,0,2,3H.05,3)
    CALL CCLTR(530.,80.,0,2,3H.06,3)
    CALL CCLTR(610.,80.,0,2,3H.07,3)
    CALL CCLTR(690.,80.,0,2,3H.08,3)
    CALL CCLTR(770.,80.,0,2,3H.09,3)
    CALL CCLTR(850.,80.,0,2,3H.10,3)
    CALL CCLTR(930.,80.,0,2,3H.11,3)
    CALL CCLTR(1010.,80.,0,2,3H.12,3)
    CALL CCLTR(43.,169.,0,2,2H20,2)
    CALL CCLTR(43.,244.,0,2,2H24,2)
    CALL CCLTR(43.,319.,0,2,2H28,2)
    CALL CCLTR(43.,394.,0,2,2H32,2)
    CALL CCLTR(43.,469.,0,2,2H36,2)
    CALL CCLTR(43.,544.,0,2,2H40,2)
    CALL CCLTR(43.,619.,0,2,2H44,2)
```

```
      CALL CCLTR(43.,694.,0,2,2H48,2)
      CALL CCLTR(43.,769.,0,2,2H52,2)
      CALL CCLTR(43.,844.,0,2,2H56,2)
      CALL CCLTR(43.,919.,0,2,2H60,2)
      CALL CCLTR(43.,994.,0,2,2H64,2)
  103 DO 104 I=1,L
      X(I)=TABLE(4,I)
      Y(I)=TABLE(3,I)
      IF(TABLE(3,I).LT.YMIN) 105,112
  112 IF(TABLE(3,I).GT.YMAX) 105,106
  105 L=I-1
      GO TO 107
  106 IF(TABLE(4,I).GT.XMAX) 105,104
  104 CONTINUE
  107 CALL CCPLOT(X,Y,L,4HJOIN)
      RETURN
      END
```

APPENDIX C

Two Surface Analysis Calculations of Martensite Habit Plane with Computer Program

The crystal shown in Fig. 9 was cut exposing the $(\bar{1}\bar{1}2)_f$ plane which is perpendicular to the $(111)_f$ plane. The exact orientation of these surfaces was obtained by back reflection Laue photographs taken at 5 cm. A third orthogonal vector is generated by taking the cross product of the vectors normal to the cut surface. The angles between the trace on each surface are measured with respect to these three orthogonal vectors, and correlated to the dot products taken between each of the three vectors and the unknown vector. This generates three equations for the vector on each of the two surfaces. The solution of these equations provides the [hkℓ] indices of the trace on each of the two surfaces. The habit plane normal is simply the cross product of these two vectors. The computer program carries out this simple calculation quickly and accurately.

The program uses a library program FLIN from the L.B.L. computer center. The deck set up is as follows:

Card 1: The number of habit planes to be calculated; I5 format.

Card 2: The normal to plane 1 and plane 2 and the measured angles between the traces on each surface. See Fig. 10 and comments in program listing; 10F8.0 format.

Card 2 is repeated the number of times specified on Card 1. The habit plane normal is printed as a unit vector. The Fortran listing follows.

```
      PROGRAM HABIT(INPUT,OUTPUT)
      COMMON/FLINC/A(40,41)
      DIMENSION B(3,4),C(3,4)
      READ 5,N
    5 FORMAT(I5)
C     N IS THE NUMBER OF DATA CARDS.
      DO 101 IA=1,N
      READ 1,((A(I,J),J=1,3),I=1,2),THETA1,THETA2,PHI1,PHI2
    1 FORMAT(10F8.0)
C     A(1,N) IS VECTOR NORMAL TO PLANE 1.  N=1,2,3
C     A(2,N) IS VECTOR NORMAL TO PLANE 2. N=1,2,3
C     PLANE 1 MUST BE 90 DEGREES FROM PLANE 2 IN THIS PROGRAM.
C     THETA1 IS ANGLE BETWEEN THE TRACE ON A(1,N) PLANE AND VECTOR A(2,N) IN DEG
C     THETA2 IS ANGLE BETWEEN THE TRACE ON A(1,N) PLANE AND VECTOR A(3,N) WHERE
C     A(3,N) IS GENERATED BY THE CROSS PRODUCT OF A(1,N) AND A(2,N).
C     PHI1 IS THE ANGLE BETWEEN THE TRACE ON A(2,N) PLANE AND A(3,N)
C     PHI2 IS THE ANGLE BETWEEN THE TRACE ON A(2,N) PLANE AND A(1,N)
      THETA1=THETA1*3.14159/180.
      THETA2=THETA2*3.14159/180.
      PHI1=PHI1*3.14159/180.
      PHI2=PHI2*3.14159/180.
C     CALCULATION OF UNIT VECTORS A(1,N) AND A(2,N).
      AB=SQRT(A(1,1)*A(1,1)+A(1,2)*A(1,2)+A(1,3)*A(1,3))
      BA=SQRT(A(2,1)*A(2,1)+A(2,2)*A(2,2)+A(2,3)*A(2,3))
      DO 102 I=1,3
      A(1,I)=A(1,I)/AB
  102 A(2,I)=A(2,I)/BA
C     CALCULATE A(3,N) VECTOR
      A(3,1)=A(1,2)*A(2,3)-A(1,3)*A(2,2)
      A(3,2)=A(1,3)*A(2,1)-A(1,1)*A(2,3)
      A(3,3)=A(1,1)*A(2,2)-A(1,2)*A(2,1)
      DO 100 I=1,3
      DO 100 J=1,3
  100 B(I,J)=A(I,J)
      A(1,4)=0.0
      A(2,4)=COS(THETA2)
      A(3,4)=COS(THETA1)
      B(1,4)=COS(PHI2)
      B(2,4)=0.0
      B(3,4)=COS(PHI1)
      PRINT 2
    2 FORMAT(39H1CALCULATION OF HKL VECTOR FOR TRACE 1.//)
      PRINT 200,((A(I,J),J=1,4),I=1,3)
      CALL FLIN(3,1,DET)
      PRINT 200,((A(I,J),J=1,4),I=1,3)
  200 FORMAT(1H0,4(E15.5,5X))
      DO 103 I=1,3
      DO 103 J=1,4
      C(I,J)=A(I,J)
  103 A(I,J)=B(I,J)
      PRINT 3
    3 FORMAT(39H0CALCULATION OF HKL VECTOR FOR TRACE 2.//)
      PRINT 200,((A(I,J),J=1,4),I=1,3)
      CALL FLIN(3,1,DET)
      PRINT 200,((A(I,J),J=1,4),I=1,3)
C     CALCULATION OF HABIT PLANE NORMAL
      ANGLE=C(1,4)*A(1,4)+C(2,4)*A(2,4)+C(3,4)*A(3,4)
```

```
      ANGLE=ACOS(ANGLE)
      ANGLE=SIN(ANGLE)
      U=(C(2,4)*A(3,4)-C(3,4)*A(2,4))/ANGLE
      V=(C(3,4)*A(1,4)-C(1,4)*A(3,4))/ANGLE
      W=(C(1,4)*A(2,4)-C(2,4)*A(1,4))/ANGLE
      AMAG=SQRT(U*U+V*V+W*W)
      U=U/AMAG
      V=V/AMAG
      W=W/AMAG
      PRINT 4,U,V,W
    4 FORMAT(19H0HABIT PLANE NORMAL,5X,2HU=,F10.5,5X,2HV=,F10.5,5X,2HW=,
     1F10.5)
  101 CONTINUE
      STOP
      END
      SUBROUTINE ERROR
      PRINT 1
    1 FORMAT(*ERROR CALLED*)
      STOP
      RETURN
      END
```

REFERENCES

1. L. Kaufman and M. Cohen, Progress in Metal Physics, Vol. 7, Pergamon Press, New York, 1958, p. 165.
2. C. L. Magee, Phase Transformations, American Society for Metals (1970), p. 115.
3. K. C. Russell, Met. Trans. 2 (1971), 5.
4. J. R. Patel and M. Cohen, Acta Met. 1 (1953), 531.
5. D. Goodchild, W. T. Roberts and D. V. Wilson, Acta Met., 18 (1970), 1151.
6. S. M. Copley, correspondence with J. Dumming, June to October, 1968.
7. J. F. Breedis, Trans. AIME, 230 (1964), 1583.
8. W. Dollasse, UCLA. Data obtained through Professor R. Wenk, Dept. of Geology, University of California, Berkeley.
9. C. Barrett and T. B. Messalski, Structure of Metals, third edition, McGraw-Hill, New York, 1966, p. 125.
10. R. Wenk, Department of Geology, University of California, Berkeley.
11. A. J. Goldman and C. N. J. Wagner, Acta Met., 11 (1963), 405.
12. W. B. Pearson, Handbook of Lattice Spacings and Structures of Metals, vol. 2, Pergamon Press, Oxford, 1967.
13. D. W. Baker, H. R. Wenk and J. M. Christie, Journal of Geology 77 (1969), 144.
14. L. G. Schulz, J. Appl. Phys., 20 (1949), 1030.
15. J. F. Breedis and W. D. Robertson, Acta Met., 10 (1962), 1077.
16. R. Lagneborg, Acta Met., 11 (1963), 11690.
17. J. A. Venables, Phil. Mag. 7 (1962), 35.
18. P. M. Kelly, Acta Met., 13 (1965), 635.

19. R. L. Patterson and C. M. Wayman, Acta Met., 14 (1966), 347.

20. B. C. Cullity, Elements of X-Ray Diffraction, Addison-Wesley, Reading, 1956, p. 398.

21. G. L. Kehl, The Principles of Metallographic Laboratory Practice, McGraw-Hill, New York, 1949, p. 413.

22. J. W. Christian, The Theory of Transformations in Metals and Alloys, Pergamon Press, Oxford, 1965, p. 809.

23. J. A. Venables, Phil. Mag., 7 (1962).

24. P. L. Manganon and G. Thomas, Met. Trans., 1 (1970), 1577.

25. J. F. Breedis and L. Kaufman, "Formation of HCP and BCC Phases in Austenitic Iron Alloys," to be published in Met. Trans.

26. S. M. Copley, and B. H. Kear, Acta Met., 16 (1968), 227.

27. J. J. Gilman, J. Appl. Phys., 36 (1965), 3195.

28. F. R. N. Nabarro, Theory of Crystal Dislocations, Clarendon Press, Oxford, 1967, p. 658.

29. G. F. Bolling and R. H. Richman, Phil. Mag., 19 (1969), 247.

30. A. Seeger, H. Kronmüller, R. Rieger and T. Träuble, J. Appl. Phys., 35 (1964), 740.

Table I. Lattice parameter measurements

		a_o*	error	a_o†	error
Fe-34.5 w/o Ni	f.c.c.	3.59168	0.00014	3.59013	0.00053
	b.c.c.	none present		2.86272	0.00197
Fe-15 w/o Ni-15 w/o Cr	f.c.c.	3.58317	0.00033	3.58560	0.00074
	b.c.c.	none present		2.86781	0.00039

*Filed at room temperature, annealed 2 hours at 850°C. Guinier method with silicon metal standard, Fe$k\alpha_1$, radiation.

†Filed at 77°K, annealed 48 hr at 275°C. Debye Scherrer method with silicon metal standard, Fe$k\alpha$ radiation.

0 0 0 0 3 6 0 5 5 7 9

Table II. The 24 variants of the Kurdjumou-Sachs orientation relationship and the 4 γ-ε interfaces. Symbols f, b, h refer to f.c.c., b.c.c. and h.c.p. crystals respectively.

Symbol	Variant		
⊡	1.	$(111)_f \| \| (110)_b$;	$[\bar{1}01]_f \| \| [\bar{1}11]_b$
	2.		$[\bar{1}01]_f \| \| [\bar{1}1\bar{1}]_b$
	3.		$[\bar{1}10]_f \| \| [\bar{1}11]_b$
	4.		$[\bar{1}10]_f \| \| [\bar{1}1\bar{1}]_b$
	5.		$[01\bar{1}]_f \| \| [\bar{1}11]_b$
	6.		$[01\bar{1}]_f \| \| [\bar{1}1\bar{1}]_b$
⊠	1.	$(\bar{1}11)_f \| \| (110)_b$;	$[\bar{1}\bar{1}0]_f \| \| [\bar{1}11]_b$
	2.		$[\bar{1}\bar{1}0]_f \| \| [\bar{1}1\bar{1}]_b$
	3.		$[\bar{1}0\bar{1}]_f \| \| [\bar{1}11]_b$
	4.		$[\bar{1}0\bar{1}]_f \| \| [\bar{1}1\bar{1}]_b$
	5.		$[01\bar{1}]_f \| \| [\bar{1}11]_b$
	6.		$[01\bar{1}]_f \| \| [\bar{1}1\bar{1}]_b$
■	1.	$(1\bar{1}1)_f \| \| (110)_b$;	$[\bar{1}01]_f \| \| [\bar{1}11]_b$
	2.		$[\bar{1}01]_f \| \| [\bar{1}1\bar{1}]_b$
	3.		$[011]_f \| \| [\bar{1}11]_b$
	4.		$[011]_f \| \| [\bar{1}1\bar{1}]_b$
	5.		$[110]_f \| \| [\bar{1}11]_b$
	6.		$[110]_f \| \| [\bar{1}1\bar{1}]_b$
⊞	1.	$(11\bar{1})_f \| \| (110)_b$;	$[011]_f \| \| [\bar{1}11]_b$
	2.		$[011]_f \| \| [\bar{1}1\bar{1}]_b$
	3.		$[\bar{1}10]_f \| \| [\bar{1}11]_b$
	4.		$[\bar{1}10]_f \| \| [\bar{1}1\bar{1}]_b$
	5.		$[101]_f \| \| [\bar{1}11]_b$
	6.		$[101]_f \| \| [\bar{1}1\bar{1}]_b$

Symbol	Variant
⊙	1. $(111)_f \| \| (0001)_h$
	2. $(1\bar{1}1)_f \| \| (0001)_h$
	3. $(\bar{1}11)_f \| \| (0001)_h$
	4. $(11\bar{1})_f \| \| (0001)_h$

Table III. The initial and final orientations of the single crystal tensile specimens. The specimen normal is near the $[111]_f$. See Fig. 1. The angles ω_1, ω_2 and ω_3 are the angles between the true specimen normal and the $[001]_f$, $[100]_f$ and $[010]_f$ poles respectively. ω_4 is the angle between the tensile axis and the $[100]_f$ pole. This data will provide a more accurate record than a plot on a unit triangle.

Initial Orientation

Alloy	tensile axis	ω_1	ω_2	ω_3	ω_4
Fe-34.5 w/o Ni	$[\bar{1}\bar{1}2]$	54.7	54.7	54.7	66.0
	$[\bar{2}\bar{1}3]$	53.0	57.0	53.0	58.0
Fe-15 w/o Ni-15 w/o Cr	$[\bar{1}\bar{1}2]$	51.5	55.0	57.0	66.5
	$[213]$	54.7	54.7	54.7	58.0

Final orientation

	tensile axis	ω_1	ω_2	ω_3	ω_4	test temperature °K	tensile strain
Fe-34.5 w/o Ni	$[\bar{1}\bar{1}2]$	56.2	52.9	52.9	71.0	273	0.0499
		55.2	53.5	53.1	71.0	178	0.0512
		53.6	53.6	54.0	71.0	121	0.0497
		53.2	54.4	54.2	69.5	77	0.0109
	$[\bar{2}\bar{1}3]$	56.0	52.7	53.0	65.0	273	0.0460
		53.5	54.5	53.7	55.5	176	0.0559
		54.8	54.5	55.2	58.5	121	0.0437
		53.2	55.0	52.9	57.0	77	0.0667
Fe-15 w/o Ni-15 w/o Cr	$[\bar{1}\bar{1}2]$	50.1	53.7	57.2	65.0	273	0.1313
		52.5	53.5	55.8	65.5	242	0.0969
		50.8	56.8	54.8	67.0	181	0.0486
	$[\bar{2}\bar{1}3]$	52.1	53.9	55.8	61.0	273	0.0515
		52.5	53.8	56.2	59.0	242	0.0994
		51.0	56.8	53.9	58.5	188	0.0514

Table IV. Habit plane measurements on $[\bar{1}\bar{1}2]_f$ specimen tested to 1% tensile strain at 77°K. The plates are numbered in Fig. 9.

Plate No.	Habit plane normal			Angle from {3 10 15}
1	-0.7850	0.5957	0.1699	4.0°
2	-0.6158	0.7663	0.1830	6.0°
3	-0.6398	0.7500	-0.1680	7.1°
4	-0.6648	0.2230	-0.7130	9.7°
5	-0.7032	0.6909	0.1680	
6	-0.73155	0.6692	-0.1306	

Table V. Summary of volume fraction measurement for Fe-34.5 w/o Ni alloy tested to 5% tensile strain at 121°K. See also Table II and Figs. 16 and 17.

Symbol	Variant		$[\bar{2}\bar{1}3]$ Tensile axis C_α	$[\bar{1}\bar{1}2]$ Tensile axis C_α
⊡2	$(111)_f \|\| (110)_b$;	$[\bar{1}01]_f \|\| [\bar{1}1\bar{1}]_b$	0.0076	0.0097
⊡4		$[\bar{1}10]_f \|\| [\bar{1}1\bar{1}]_b$	0.0052	0.0142
⊡6		$[01\bar{1}]_f \|\| [\bar{1}1\bar{1}]_b$	0.0804	0.0458
⊠1	$(\bar{1}11)_f \|\| (110)_b$;	$[\bar{1}\bar{1}0]_f \|\| [\bar{1}11]_b$	<0.0005	0.0073
⊠2		$[\bar{1}\bar{1}0]_f \|\| [\bar{1}1\bar{1}]_b$	0.0070	0.0130
⊠3		$[\bar{1}0\bar{1}]_f \|\| [\bar{1}11]_b$	not observed	0.0050
■2	$(1\bar{1}1)_f \|\| (110)_b$;	$[\bar{1}01]_f \|\| [\bar{1}1\bar{1}]_b$	0.0008	not observed
■4		$[011]_f \|\| [\bar{1}1\bar{1}]_b$	not observed	0.0008
■5		$[110]_f \|\| [\bar{1}11]_b$	not observed	0.0037
■6		$[110]_f \|\| [\bar{1}1\bar{1}]_b$	0.0013	0.0029
⊞1	$(11\bar{1})_f \|\| (110)_b$;	$[011]_f \|\| [\bar{1}11]_b$	0.0026	0.0031
⊞2		$[011]_f \|\| [\bar{1}1\bar{1}]_b$	not observed	0.0002
⊞3		$[\bar{1}10]_f \|\| [\bar{1}11]_b$	0.0013	0.0039
		Total	0.1067	0.1096

Table VI. Summary of volume fraction measurements for Fe-15 w/o Ni-15 w/o Cr alloy tested to 5% tensile strain at 185°K. See also Table II and Figs. 18 and 19.

Symbol	Variant		$[\bar{2}\bar{1}3]$ Tensile axis C_α and C_ε	$[\bar{1}\bar{1}2]$ Tensile axis C_α and C_ε
⊠ 1	$(\bar{1}11)_f \|\| (110)_b$;	$[\bar{1}\bar{1}0]_f \|\| [\bar{1}11]_b$	0.0072	0.0018
⊠ 2		$[\bar{1}\bar{1}0]_f \|\| [\bar{1}1\bar{1}]_b$	0.0033	<0.0006
⊠ 3		$[\bar{1}0\bar{1}]_f \|\| [\bar{1}11]_b$	0.0011	not observed
⊠ 5		$[01\bar{1}]_f \|\| [\bar{1}11]_b$	0.0137	0.0006
⊠ 6		$[01\bar{1}]_f \|\| [\bar{1}1\bar{1}]_b$	0.0421	0.0019
■ 1	$(1\bar{1}1)_f \|\| (110)_b$;	$[\bar{1}01]_f \|\| [\bar{1}11]_b$	not observed	0.0132
■ 2		$[\bar{1}01]_f \|\| [\bar{1}1\bar{1}]_b$	not observed	0.0056
■ 5		$[110]_f \|\| [\bar{1}11]_b$	not observed	0.0020
■ 6		$[110]_f \|\| [\bar{1}1\bar{1}]_b$	not observed	0.0041
⊙ 2	$(1\bar{1}1)_f \|\| (0001)_h$		not observed	0.0194
⊙ 3	$(\bar{1}11)_f \|\| (0001)_h$		0.0214	0.0091
		Total	0.0888	0.0583

INPUT DATA

SPECIMEN FE-15NI-15CR, CUT NO, 11, TENSILE AXIS 123 , TEST DATE 5/1/70
TEST TEMPERATURE 242 DEGREES KELVIN.

.0500 5.0 CROSSHEAD SPEED AND CHART SPEED, UNITS CM/MIN.
19.05003.65401.6420 GAUGE LENGTH, WIDTH AND THICKNESS, UNITS MM.
52.0 40.0 PHI AND LAMBDA, UNITS DEGREES
100 INSTRON LOAD SCALE, UNITS KG.
1 KEY=1 INPUT UNITS ARE KG, CM, AND MM.

69.9	11.1	71.2	11.5	71.8	11.7	71.2	12.5	70.8	13.5	70.0	14.5
70.6	16.5	70.6	18.5	70.5	20.5	70.6	25.5	70.7	30.5	70.9	35.5
71.0	40.5	71.0	45.5	71.1	50.5	71.2	55.5	71.3	57.7	60.0	55.3
68.0	57.5	71.0	58.5	71.6	58.9	71.8	59.5	71.9	61.5	72.0	63.5
72.1	65.5	72.2	67.5	72.3	70.5	72.8	75.5	73.2	80.5	73.5	85.5
74.0	90.5	74.4	95.5	74.8	100.5	75.3	106.7	-70.0	104.5	-999.0	-0.

OUTPUT DATA

STRAIN RATE= .02625 PER MIN. SHEAR STRAIN RATE= .04263 PER MIN.

LOAD KG	CHANGE IN LENGTH MM	STRESS KG/MM**2	STRAIN	SHEAR STRESS KG/MM**2	SHEAR STRAIN
69.90	.0000	11.650	.00000	7.173	0.
71.20	.0039	11.867	.00020	7.306	.00033
71.80	.0060	11.967	.00031	7.368	.00051
71.20	.0239	11.867	.00125	7.306	.00204
70.80	.0451	11.800	.00237	7.265	.00385
70.00	.0677	11.667	.00355	7.183	.00577
70.60	.1058	11.767	.00555	7.244	.00902
70.60	.1458	11.767	.00765	7.244	.01243
70.50	.1861	11.750	.00977	7.234	.01587
70.60	.2858	11.767	.01500	7.244	.02437
70.70	.3855	11.784	.02023	7.255	.03287
70.90	.4848	11.817	.02545	7.275	.04134
71.00	.5845	11.834	.03068	7.285	.04984
71.00	.6845	11.834	.03593	7.285	.05836
71.10	.7842	11.850	.04116	7.296	.06686
71.20	.8839	11.867	.04640	7.306	.07536
71.30	.9276	11.884	.04869	7.316	.07909
60.00	.9154	10.000	.04805	6.157	.07805
68.00	.9340	11.334	.04903	6.978	.07964
71.00	.9445	11.834	.04958	7.285	.08053
71.60	.9506	11.934	.04990	7.347	.08105
71.80	.9620	11.967	.05050	7.368	.08202
71.90	1.0016	11.984	.05258	7.378	.08540
72.00	1.0413	12.000	.05466	7.388	.08879
72.10	1.0810	12.017	.05675	7.398	.09217
72.20	1.1207	12.034	.05883	7.409	.09555
72.30	1.1804	12.050	.06196	7.419	.10064
72.80	1.2788	12.134	.06713	7.470	.10903
73.20	1.3775	12.200	.07231	7.511	.11745
73.50	1.4766	12.250	.07751	7.542	.12590
74.00	1.5750	12.334	.08268	7.593	.13429
74.40	1.6737	12.400	.08786	7.634	.14271

FIGURE CAPTIONS

Fig. 1. The single crystal tensile specimen showing the crystal orientation and the final dimensions after electropolishing.

Fig. 2. Geometry of the pole figure goniometer. The diagram illustrates a specimen in the reflection position. The collimator (col.), primary beam, and scintillation counter (s.c.) are stationary. In reflection the specimen is rotated about axes B (fixed) and A (rotated about B); A is the specimen normal. Only lattice planes with poles parallel to OP are recored. After Baker et al.[13]

Fig. 3. Sterographic plot showing the position of the {002} poles for each of the 24 K-S variants in a $(111)_f$ single crystal matrix. See Table 11 for code of symbols.

Fig. 4. Stereographic plot showing the position of the $\{10\bar{1}1\}_h$ poles for the γ-ε variants of the orientation relation in a $(111)_f$ single crystal matrix. See Table II for code of symbols.

Fig. 5. Fe-34.5 w/o Ni $[\bar{1}\bar{1}2]$ tensile axis stress strain data. Arrow indicates specimen was unloaded.

Fig. 6. Fe-34.5 w/o Ni $[\bar{2}\bar{1}3]$ tensile axis stress strain data. Arrow indicates specimen was unloaded.

Fig. 7. Slip line structure of Fe-34.5 w/o alloy single slip specimen tested at 273°K.

Fig. 8. Typical microstructure of duplex slip Fe-34.5 w/o alloy specimen tested at 121°K. See Table IV and Appendix C.

Fig. 9. Optical micrographs showing details of two surface analysis performed on the duplex slip Fe-34.5 w/o Ni alloy specimen tested to 1% tensile strain at 77°K.

Fig. 10. Fe-15 w/o Ni-15 w/o Cr $[\bar{1}\bar{1}2]$ tensile axis stress strain data. Arrow indicates specimen was unloaded.

Fig. 11. Fe-15 w/o Ni-15 w/o Cr $[\bar{2}\bar{1}3]$ tensile axis stress strain data. Arrow indicates specimen was unloaded.

Fig. 12. Slip line structure and surface martensite in a Fe-15 w/o Ni-15 w/o Cr alloy duplex slip specimen tested at 273°K.

Fig. 13. Etched surface showing ε martensite in a Fe-15 w/o Ni-15 w/o Cr alloy duplex slip specimen tested at 242°K.

Fig. 14. Microstructure of deformation induced transformation in Fe-15 w/o Ni-15 w/o Cr alloy single slip specimen A and duplex slip specimen B tested at 185°K.

Fig. 15. Polish and etch experiment of Fe-15 w/o Ni-15 w/o Cr alloy single slip specimen, tested at 188°K, showing martensite observed on the surface is bulk martensite. Plate A is the as tested surface, plate B was electropolished removing 0.002 mm from the surface, and plate C was etched.

Fig. 16. Experimentally observed K-S variants for the Fe-34.5 w/o $[\bar{2}\bar{1}3]_f$ tensile axis specimen tested to 5% tensile strain at 121°K. See Table V.

Fig. 17. Experimentally observed K-S variants for the Fe-34.5 w/o $[\bar{1}\bar{1}2]_f$ tensile axis specimen tested to 5% tensile strain at 121°K. See Table V.

Fig. 18. Experimentally observed K-S variants for the Fe-15 w/o Ni-15 w/o Cr $[\bar{2}\bar{1}3]$ tensile axis specimen tested to 5% tensile strain at 188°K. See Table VI.

Fig. 19. Experimentally observed K-S variants for the Fe-15 w/o Ni-15 w/o Cr $[\bar{1}\bar{1}2]$ tensile axis specimen tested to 5% tensile strain at 181°K. See Table VI.

Fig. 20. Plot of the temperature dependence of the flow stress for easy glide for both alloys studied.

Fig. 21. Plot showing dynamic separation of partial dislocations as a function of resolved shear stress on the following and leading partials. After Copley and Kear.[26]

Fig. 22. Electron micrograph showing the presence of both twinned and dislocated martensite of the same crystal orientation. A shows a fully twinned segment of a single plate which has a partially twinned and dislocated region. B is a fully twinned martensite plate.

0 0 0 0 3 6 0 6 5 8 4

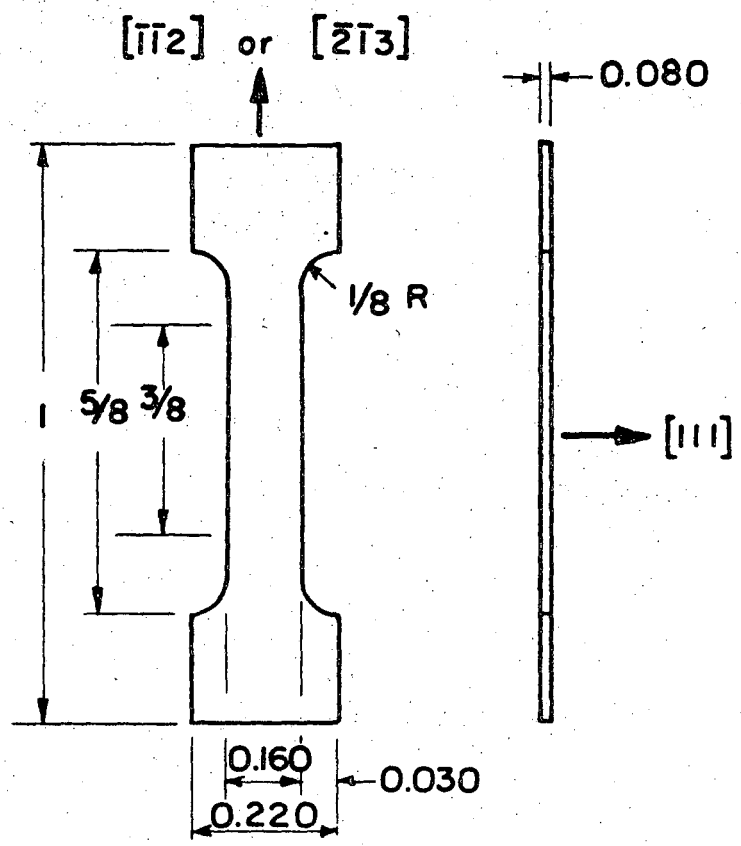

XBL718-7094

Fig. 1.

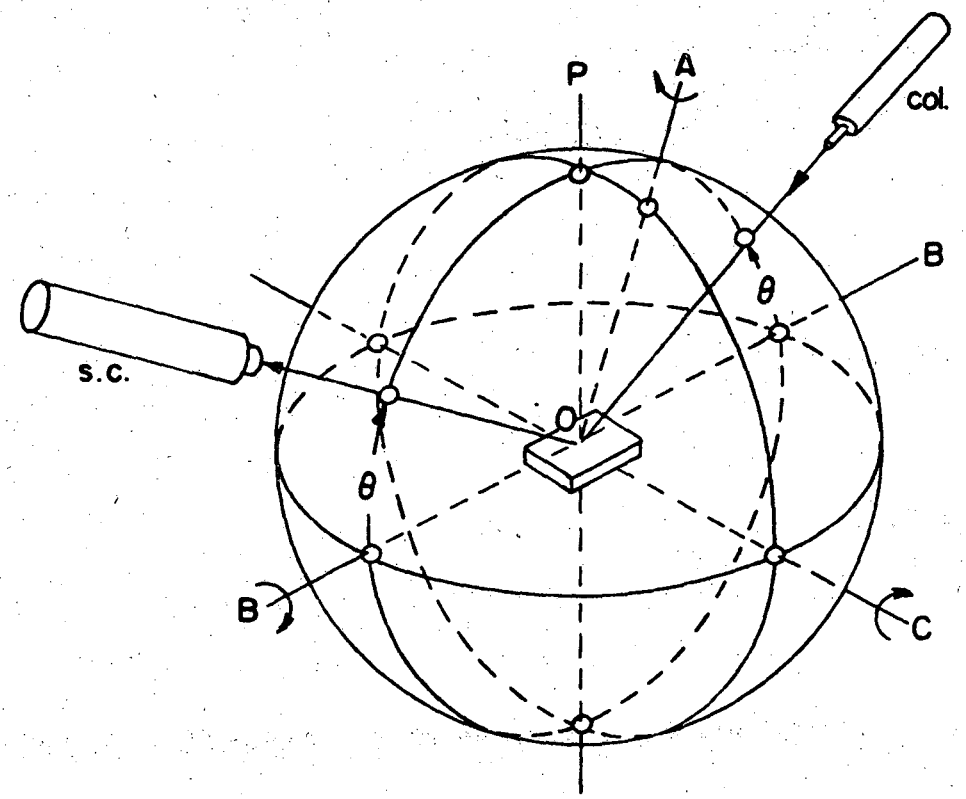

XBL718-7095

Fig. 2.

0 0 0 0 3 6 0 0 5 8 5

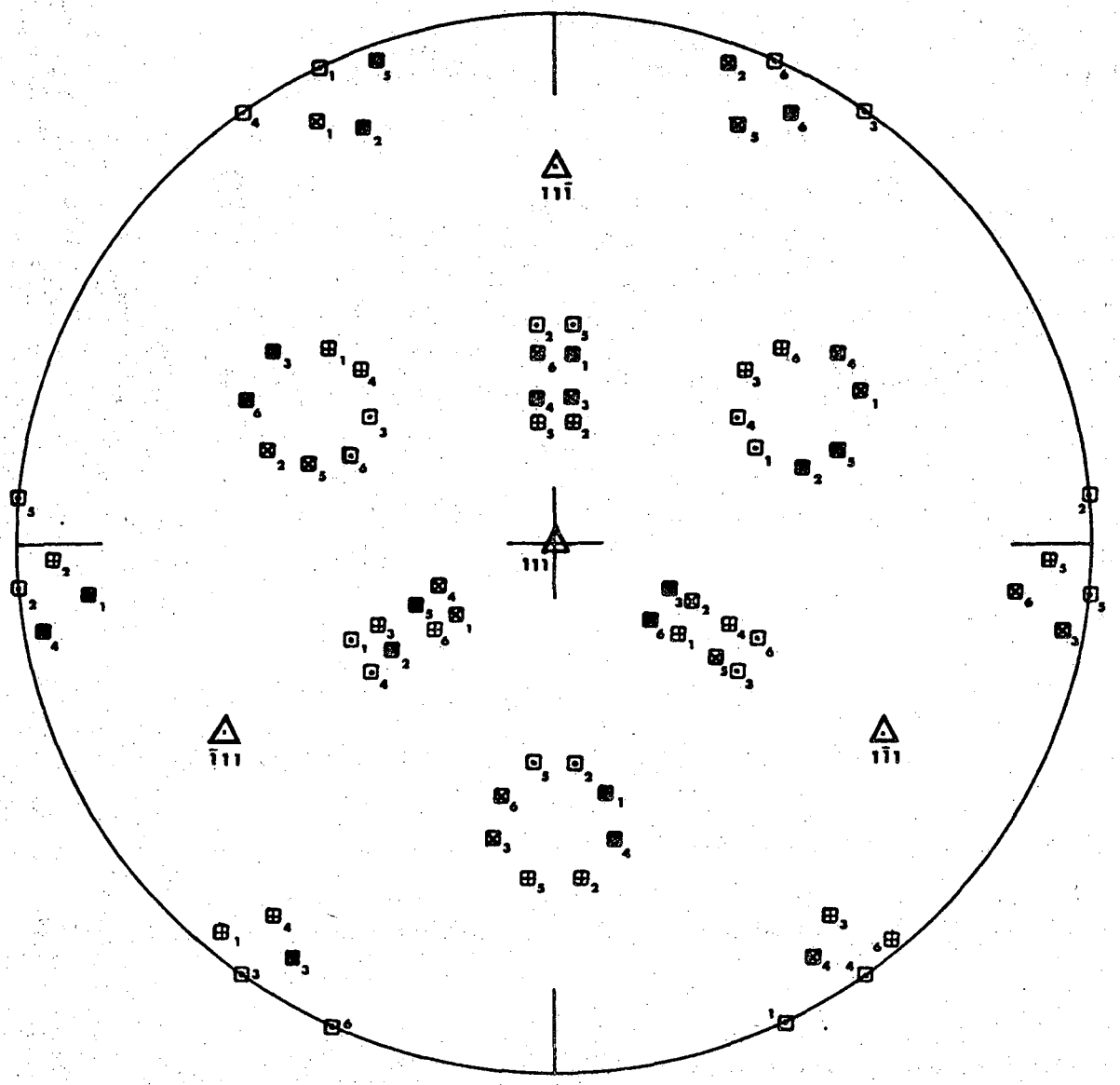

XBL 7011-7050

Fig. 3.

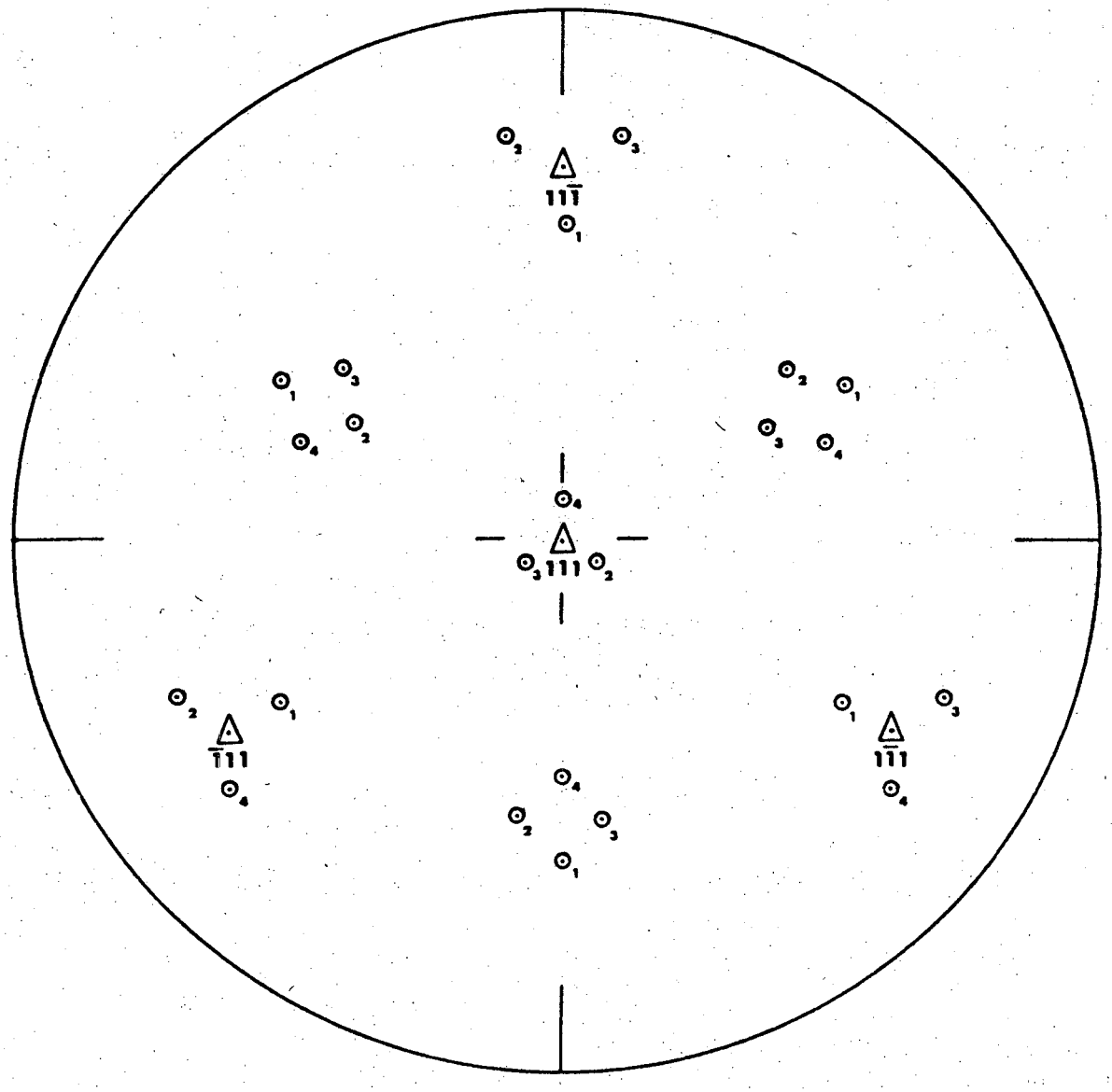

XBL 717-7072

Fig. 4.

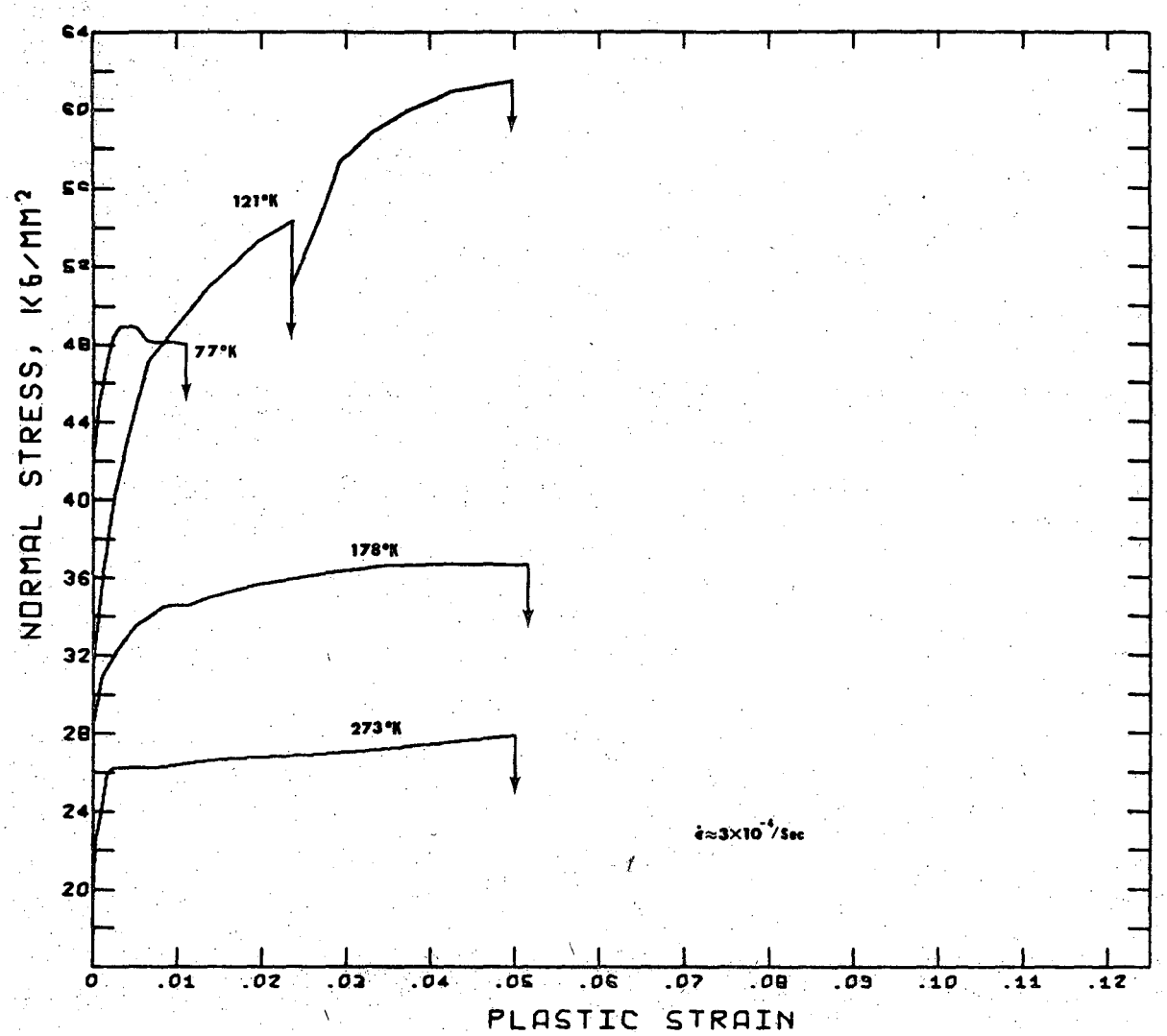

XBL 7011-6955

Fig. 5.

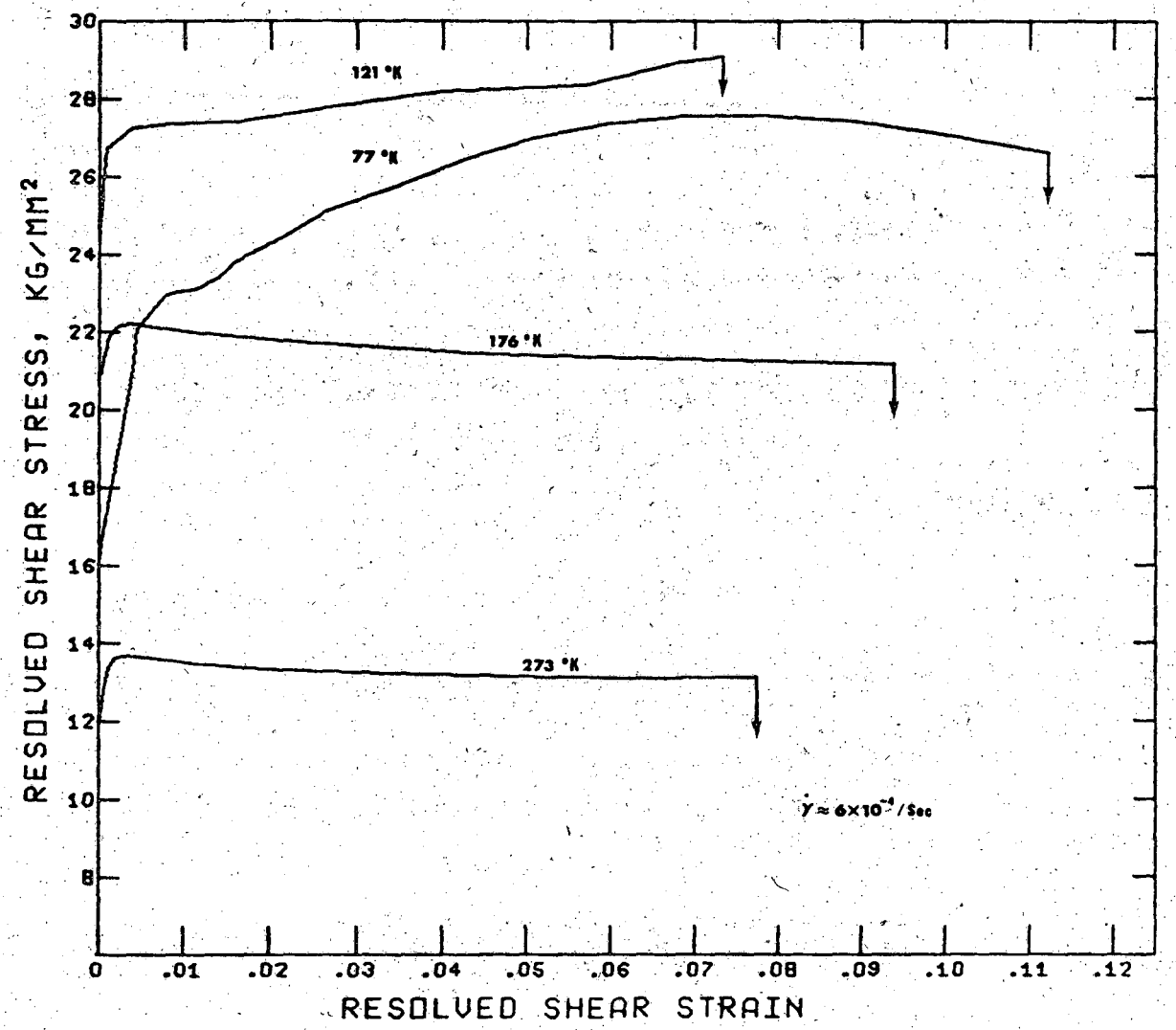

XBL 7011-6954

Fig. 6.

0 0 0 0 3 6 0 6 5 8 7

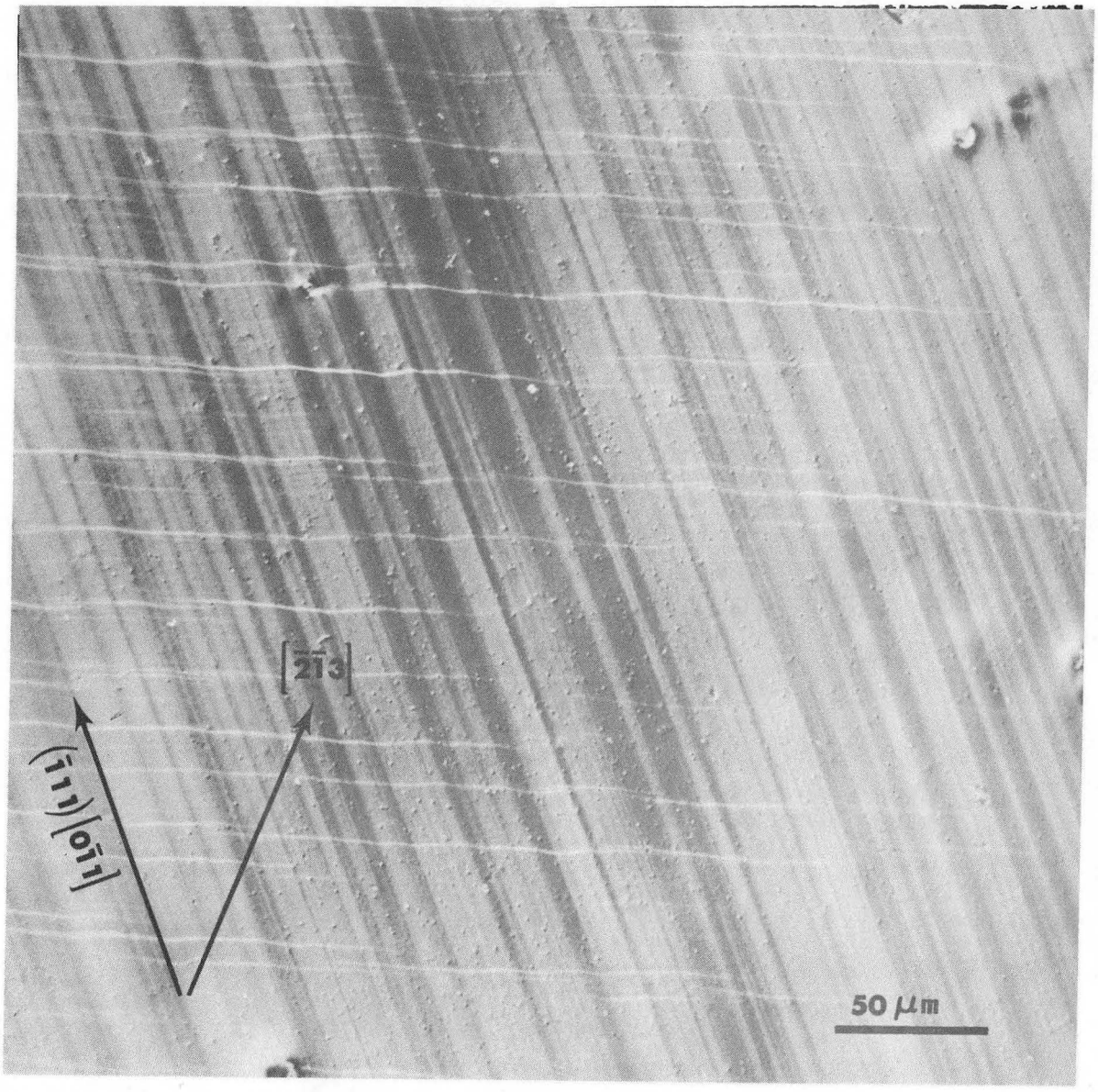

XBB 717-3417

Fig. 7.

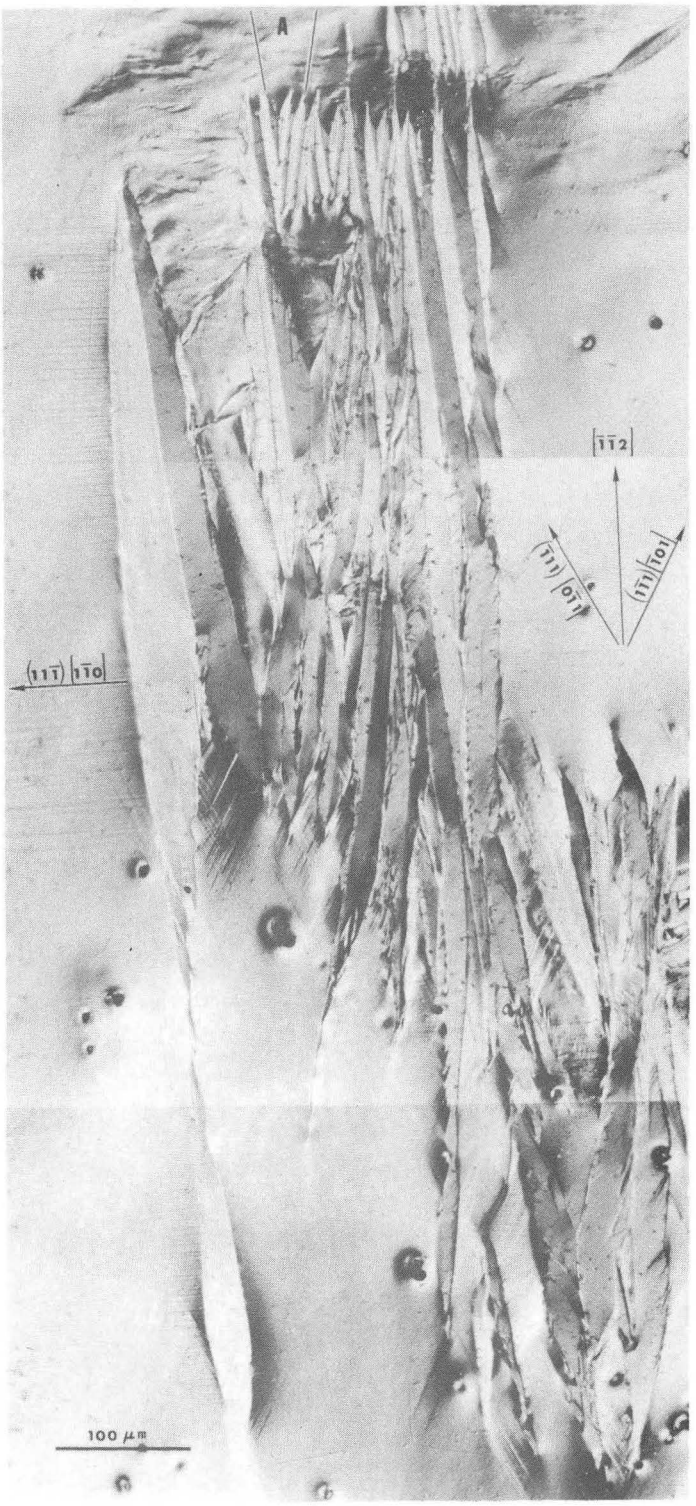

XBB 7012-5470

Fig. 8.

0 0 0 0 3 6 0 0 3 8 8

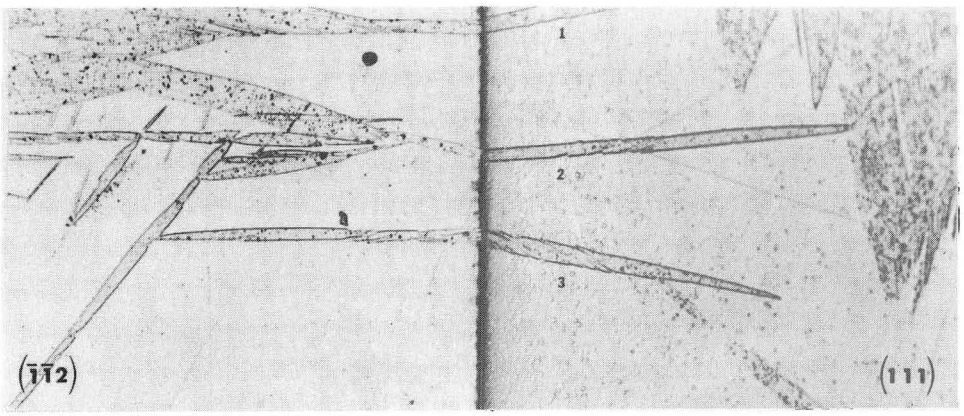

A

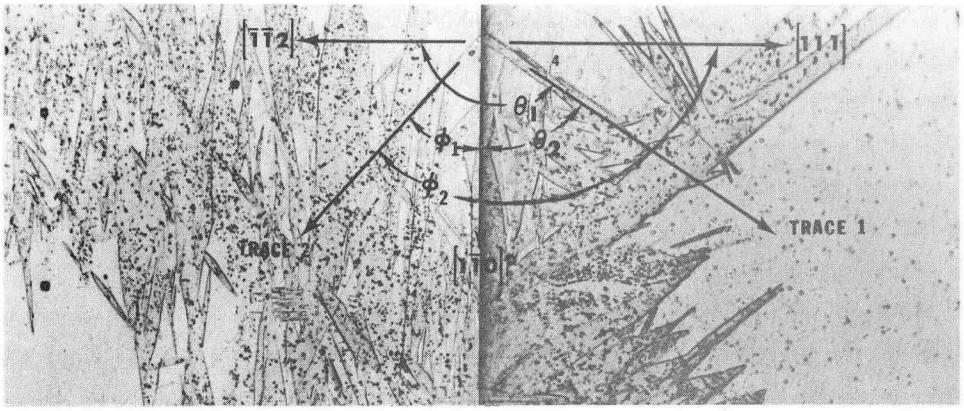

B

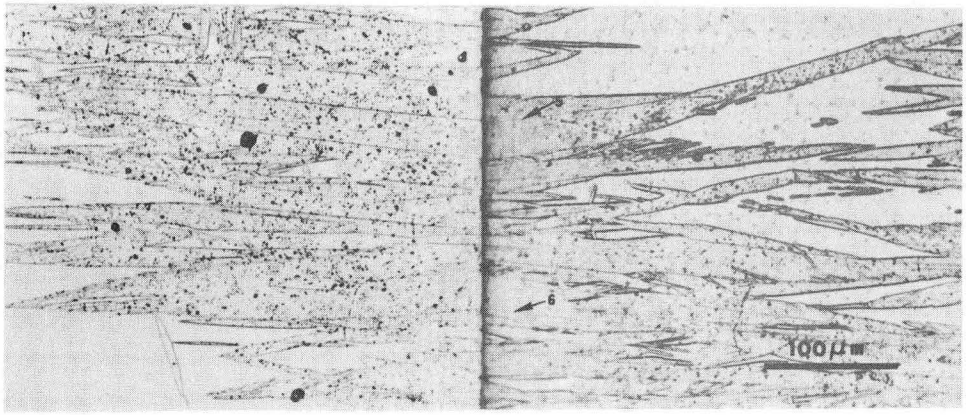

C

XBB 717-3416

Fig. 9.

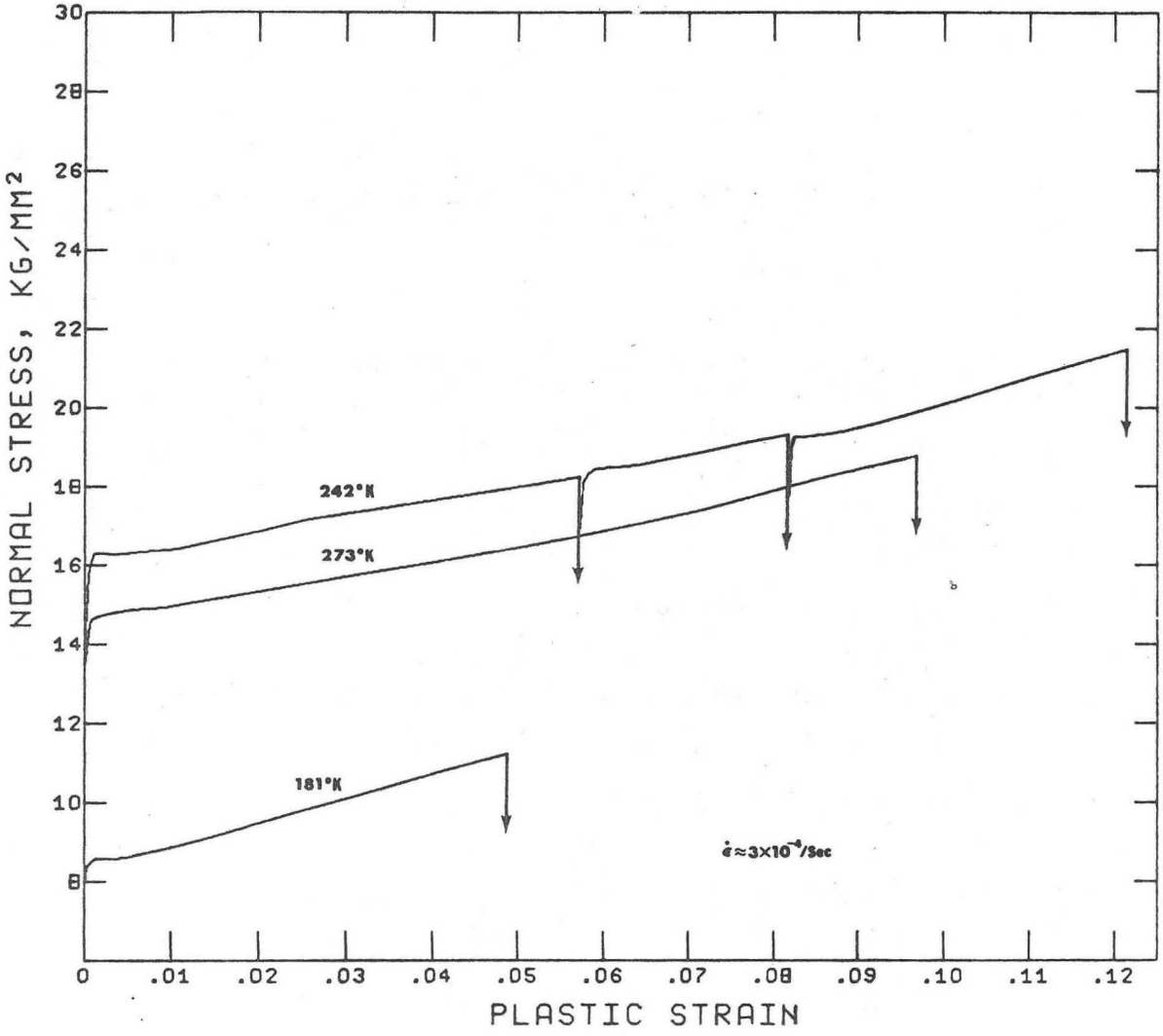

XBL 7011-6953

Fig. 10.

0 0 0 0 3 6 0 0 3 8 9

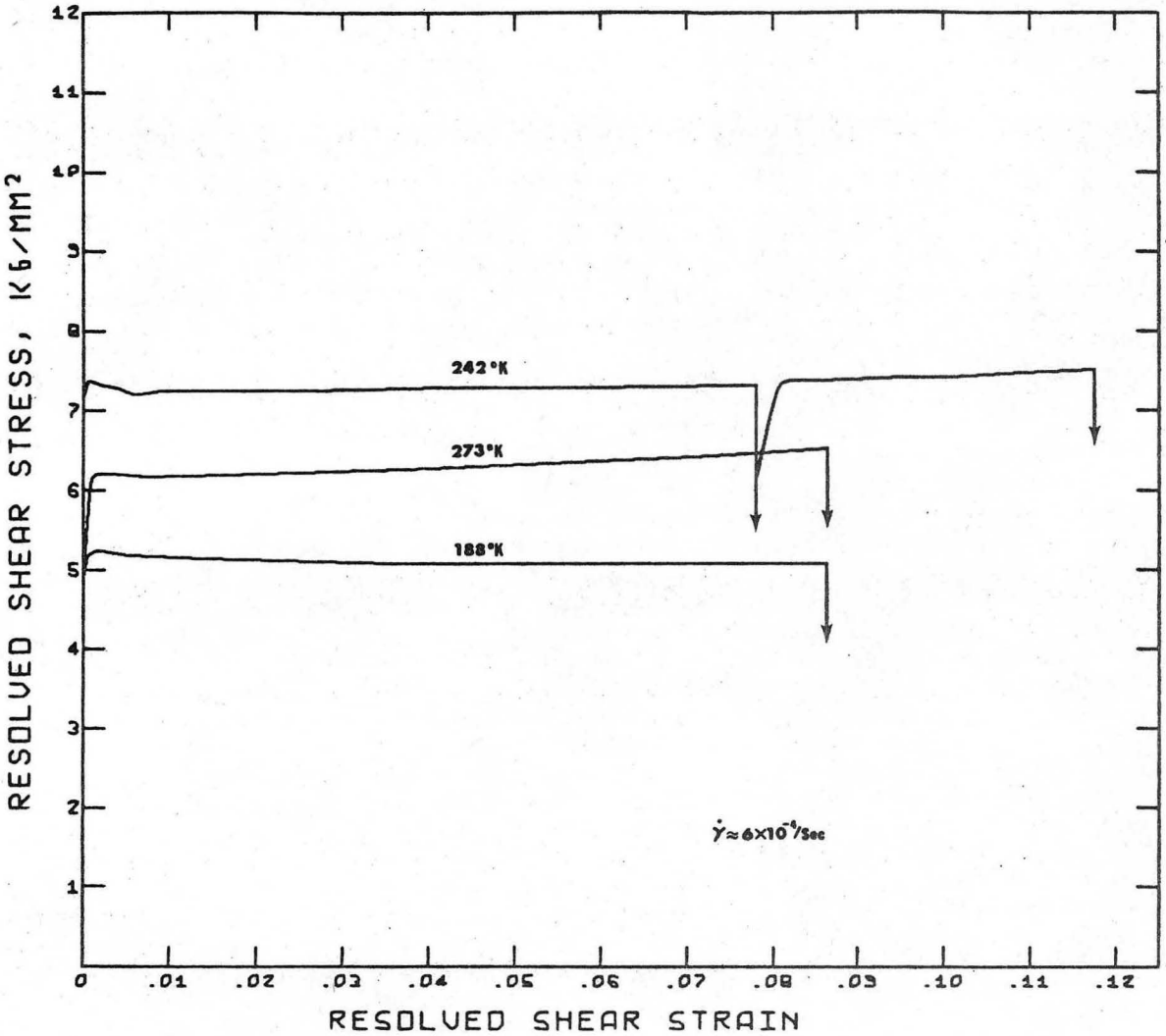

XBL 7011-6956

Fig. 11.

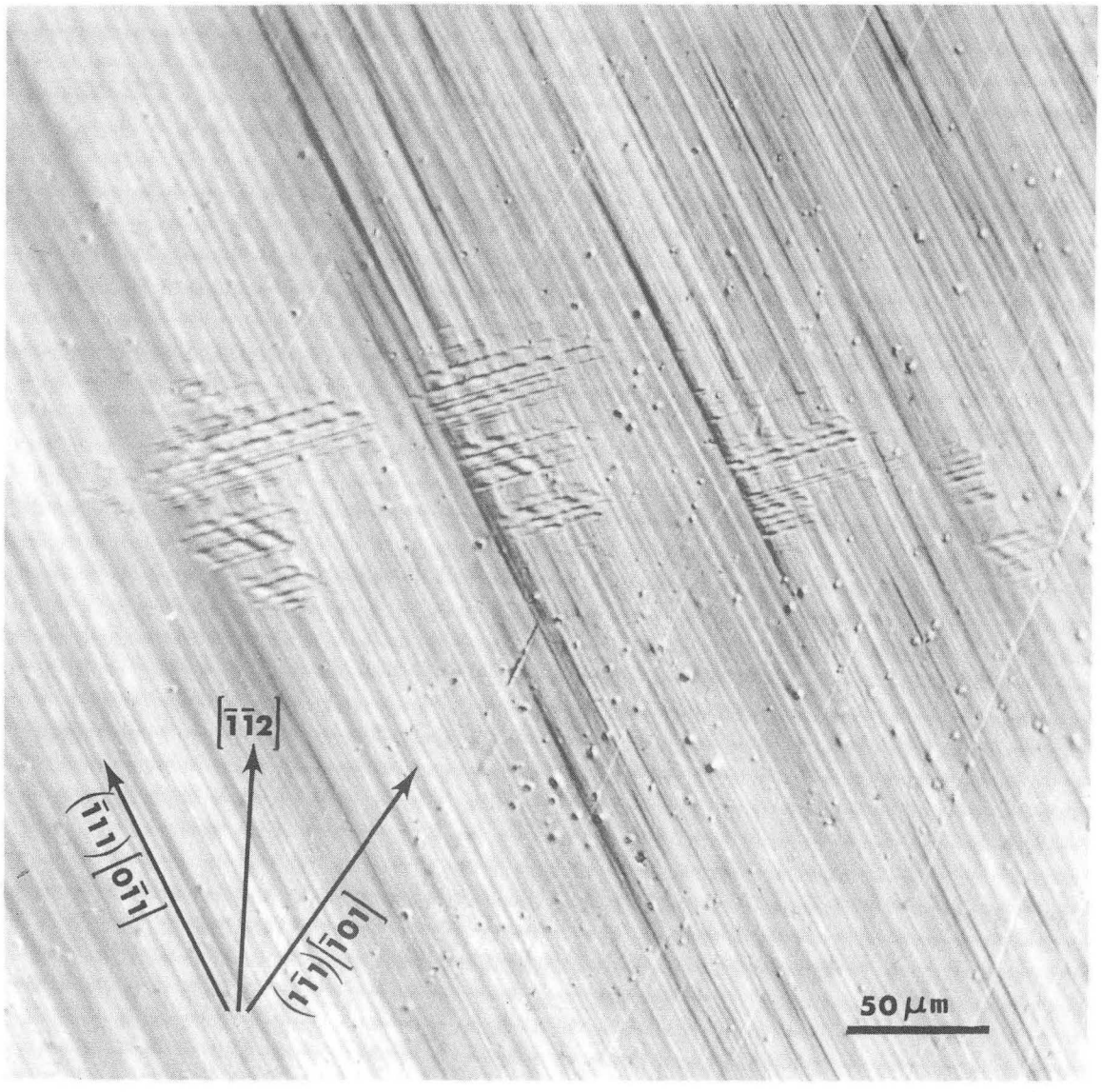

XBB 717-3419

Fig. 12.

0 0 0 0 3 6 0 5 5 9 0

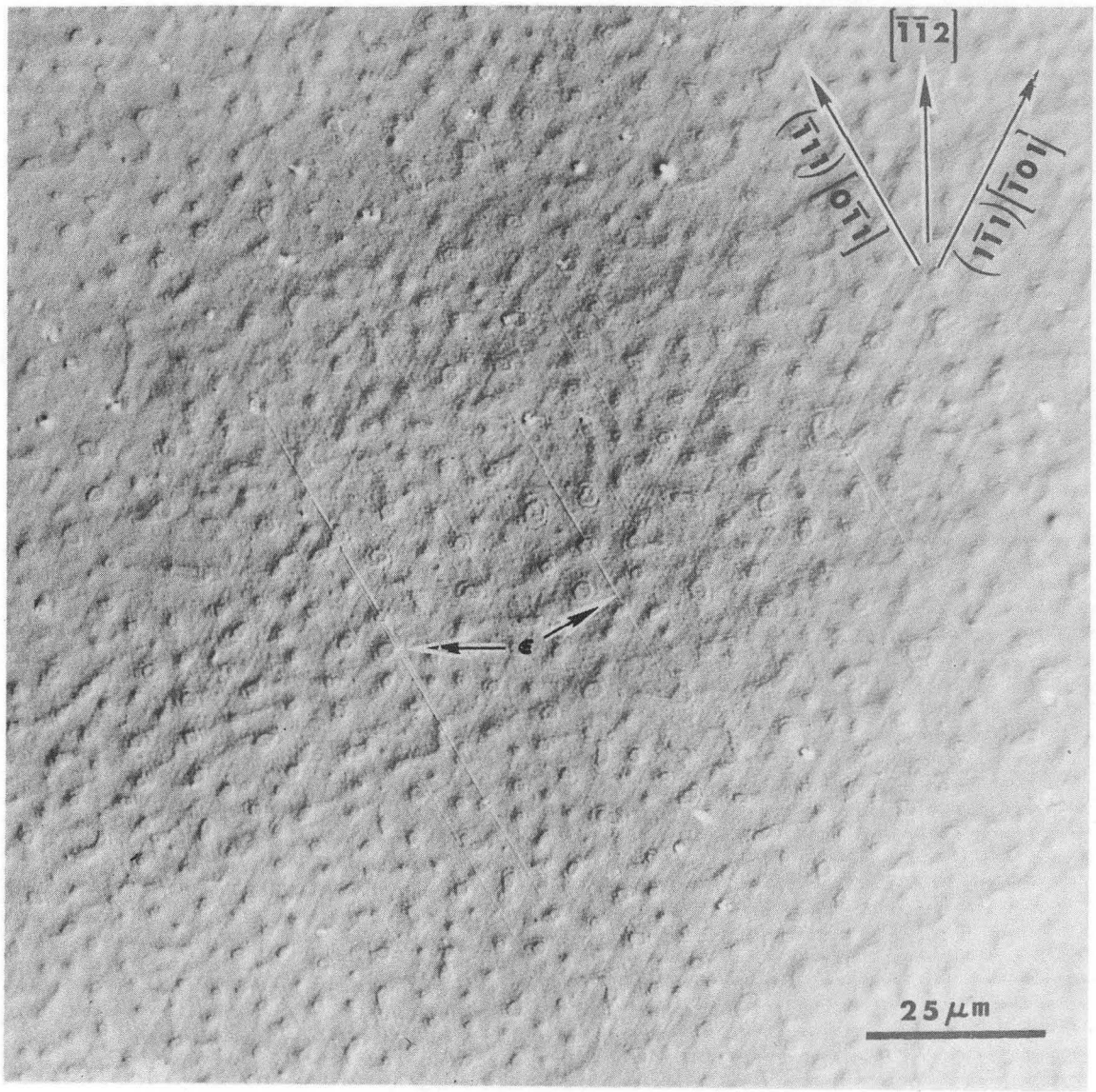

XBB 717-3418

Fig. 13.

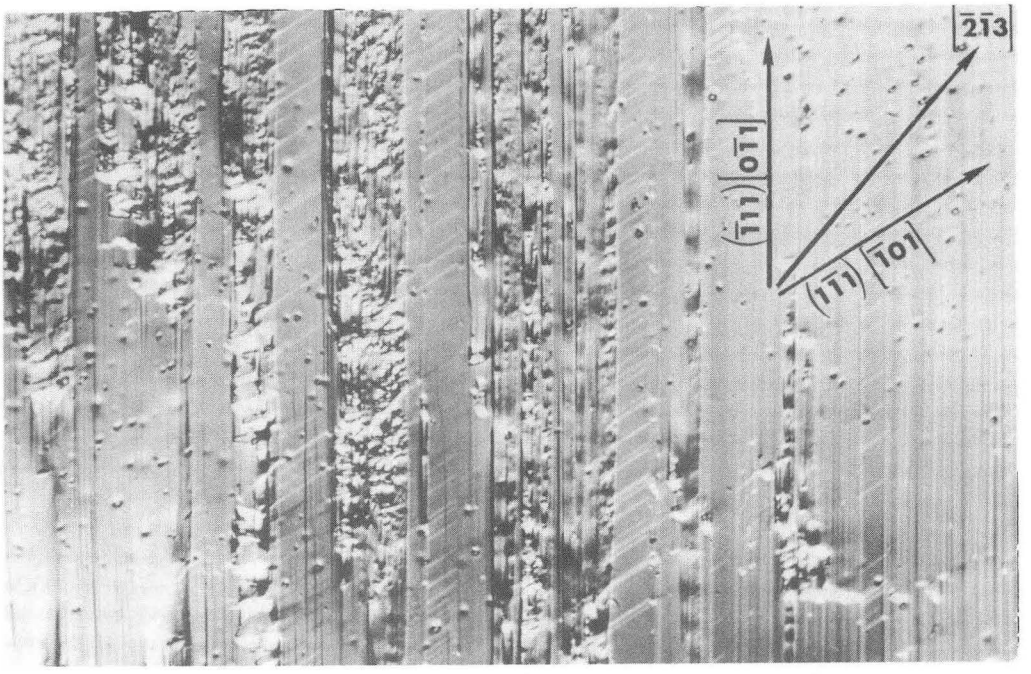

A

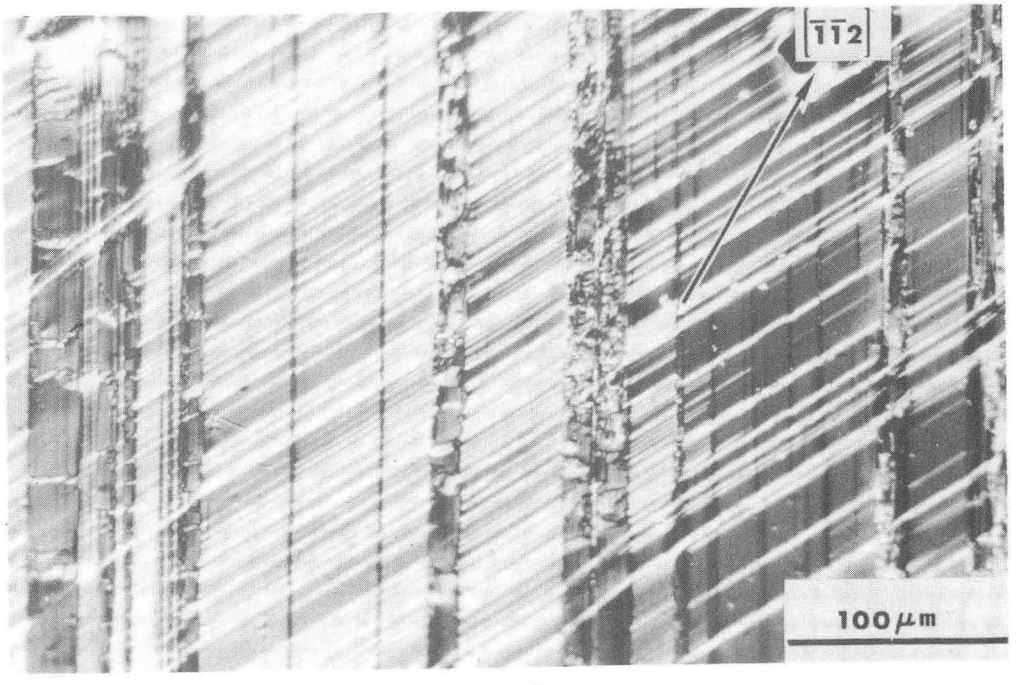

B

XBB 7012-5468

Fig. 14.

0 0 0 0 3 6 0 0 5 9 1

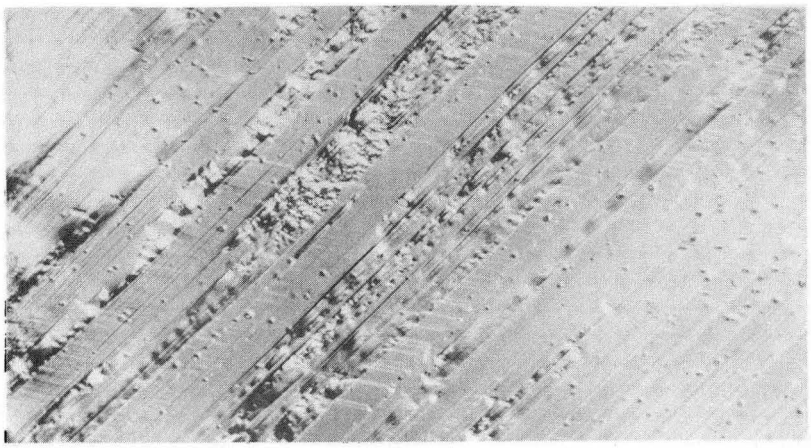

A

B

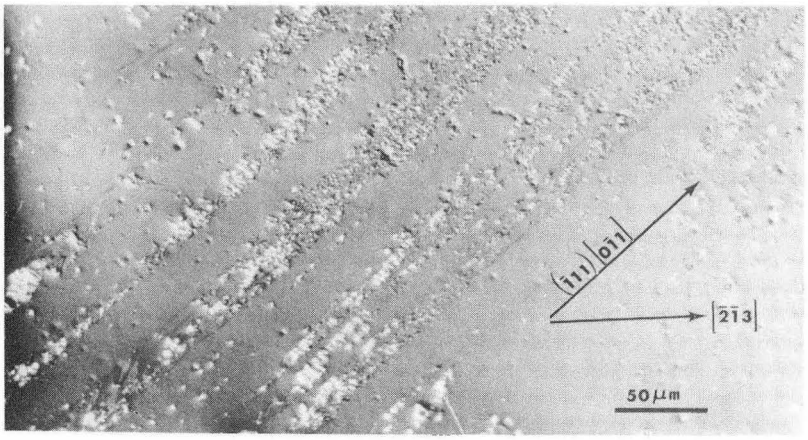

C XBB 717-3415

Fig. 15.

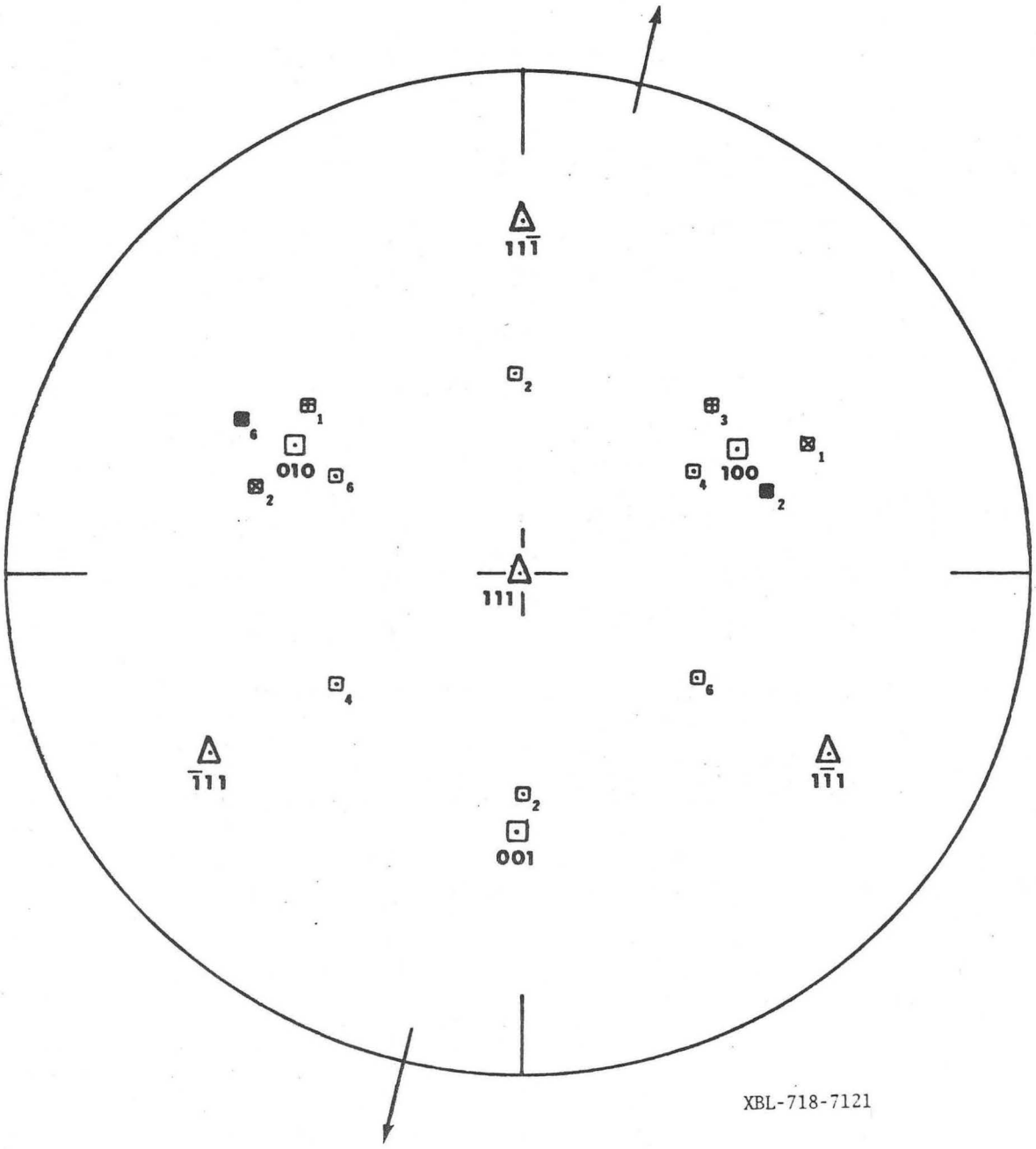

Fig. 16.

0 0 0 0 3 6 0 5 3 9 2

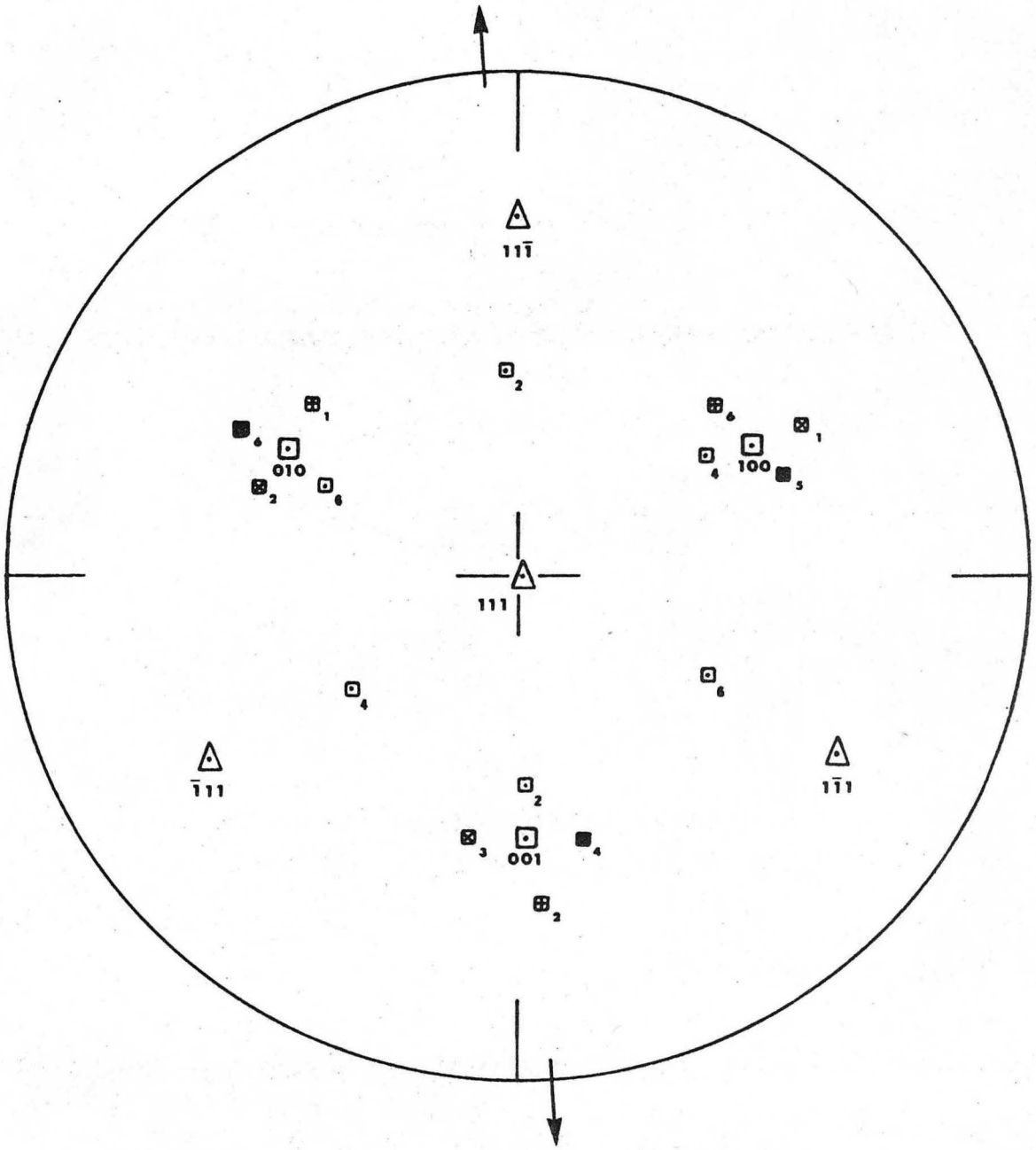

XBL 717-7070

Fig. 17.

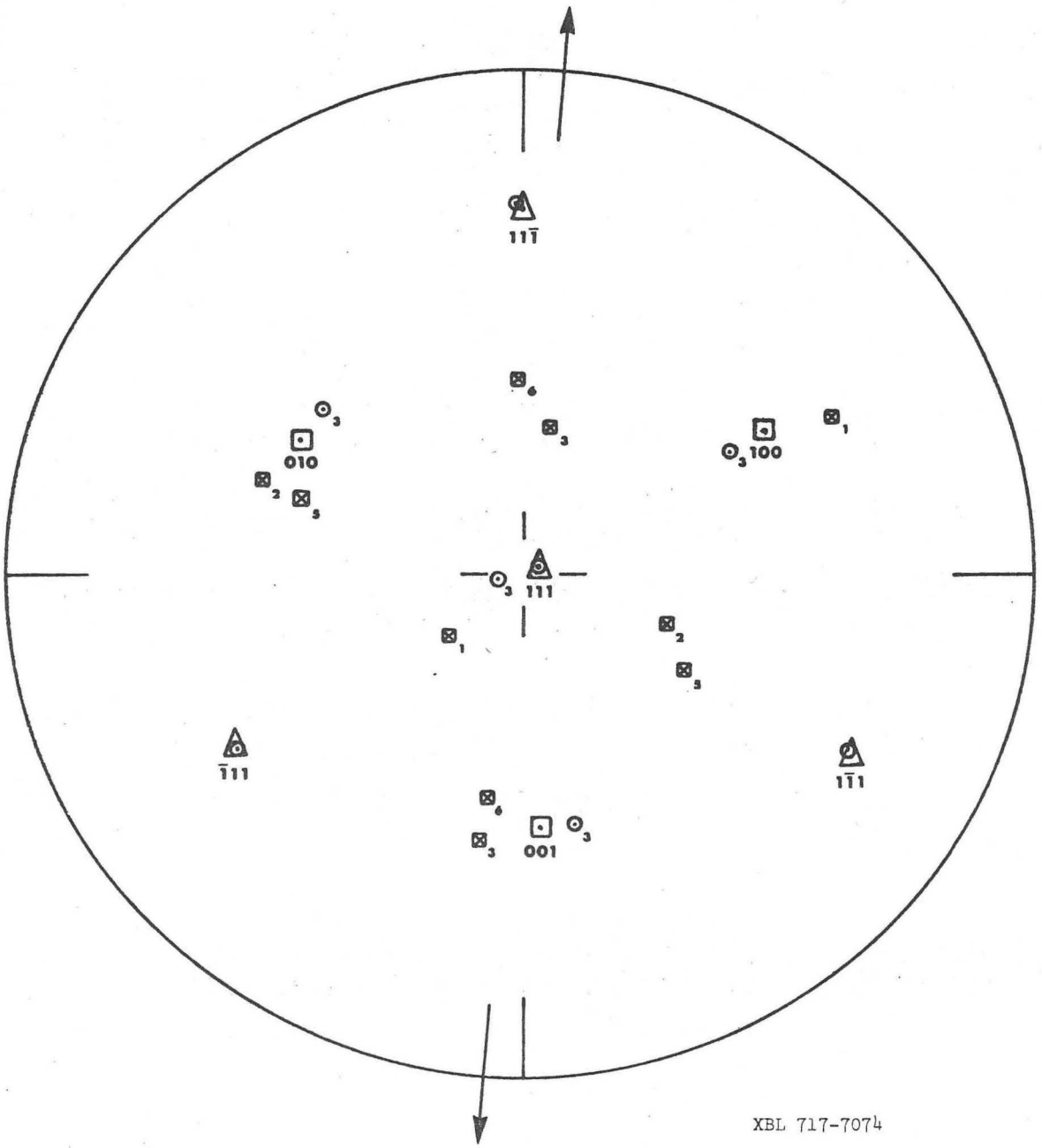

XBL 717-7074

Fig. 18.

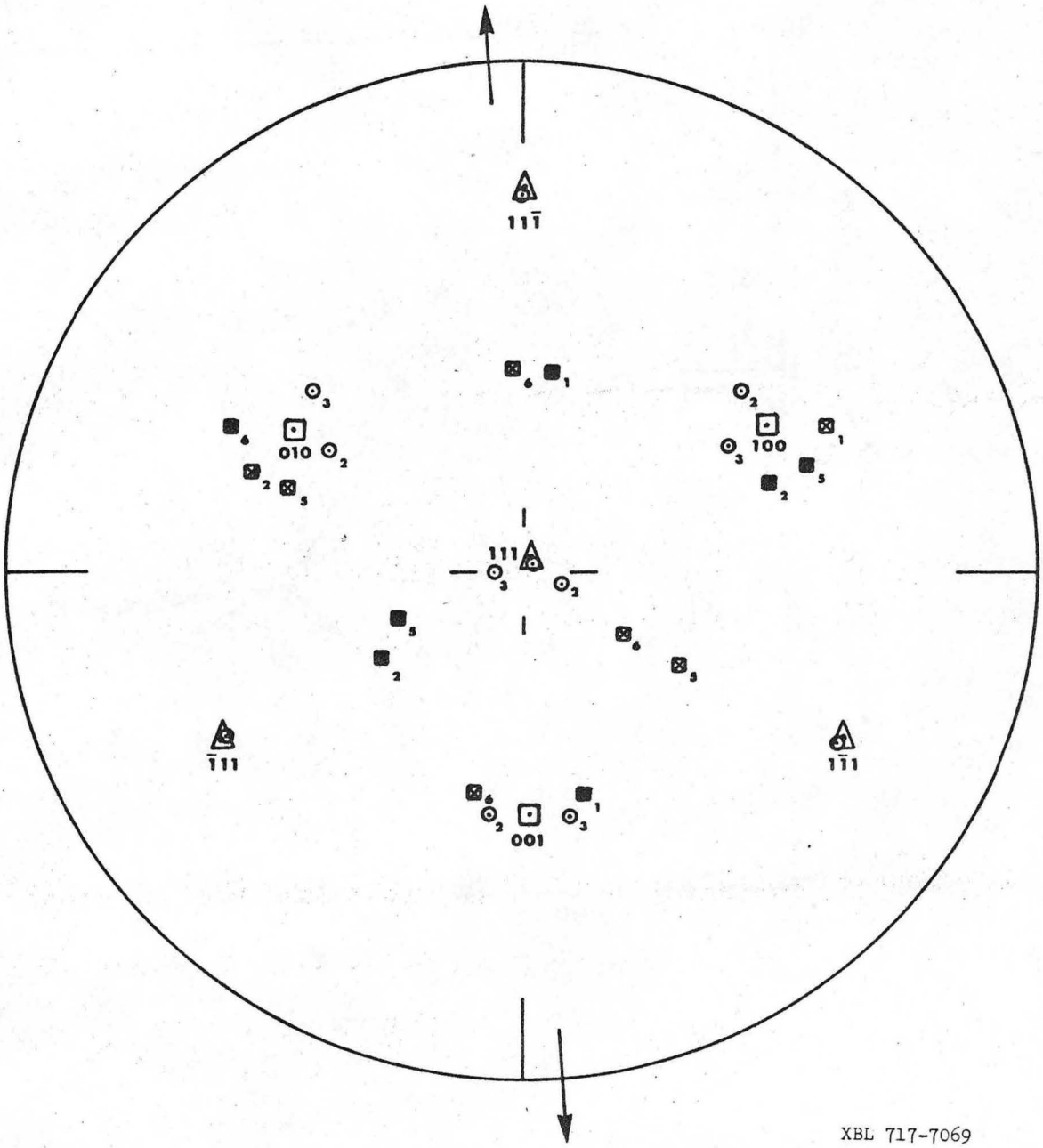

XBL 717-7069

Fig. 19.

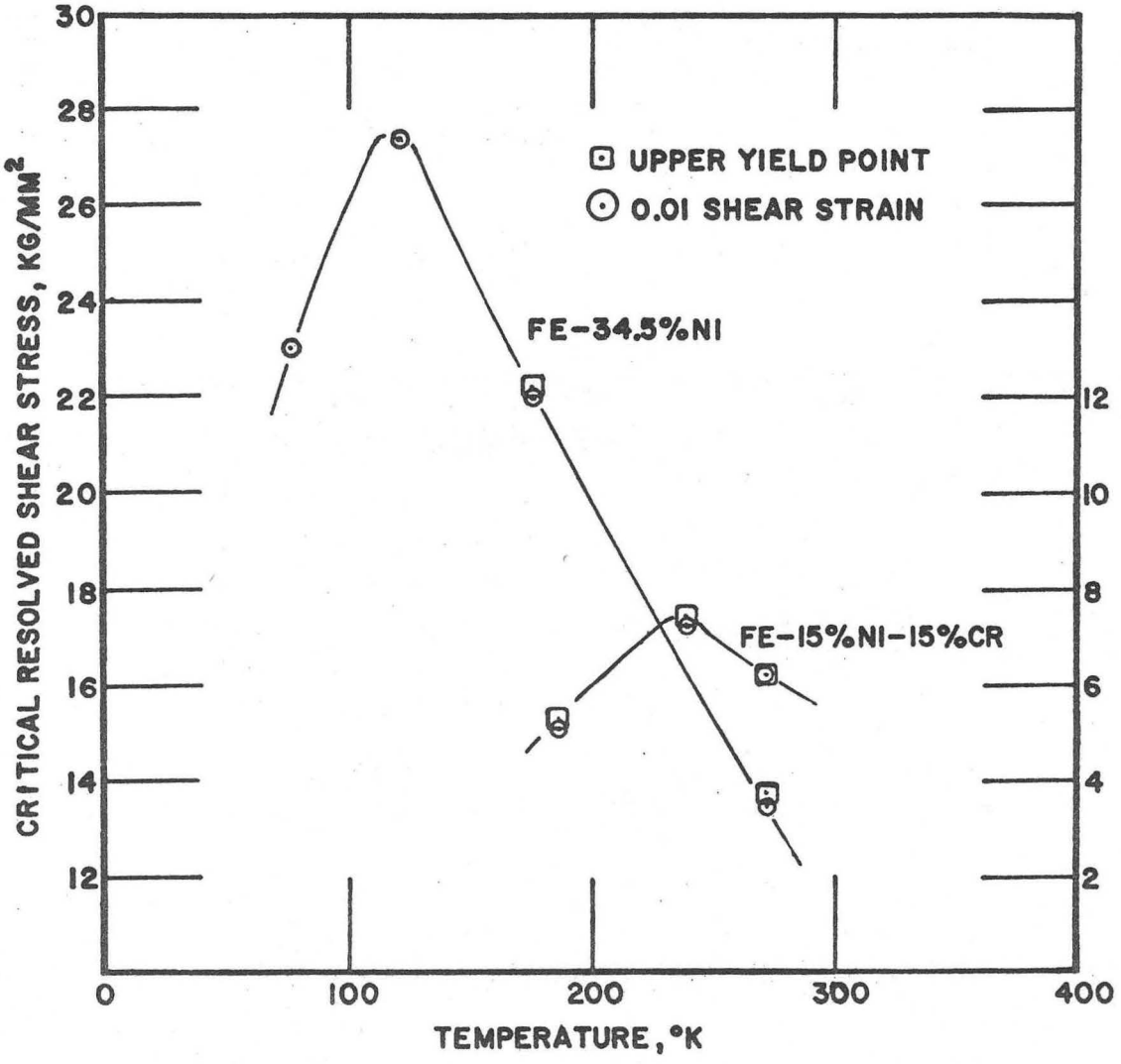

XBL 717-7071

Fig. 20.

0 0 0 0 3 6 0 0 3 9 3

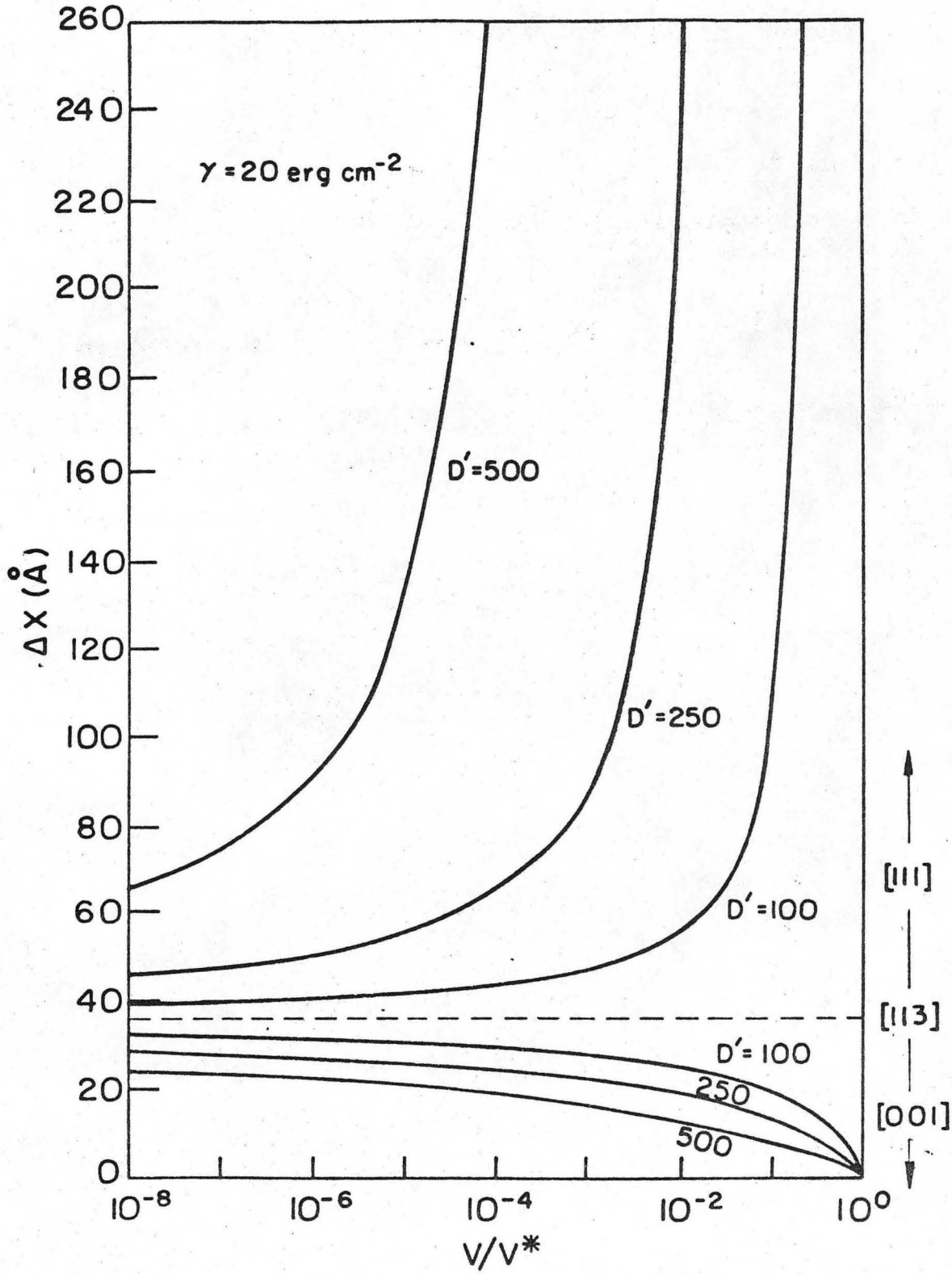

XBL718-7093

Fig. 21.

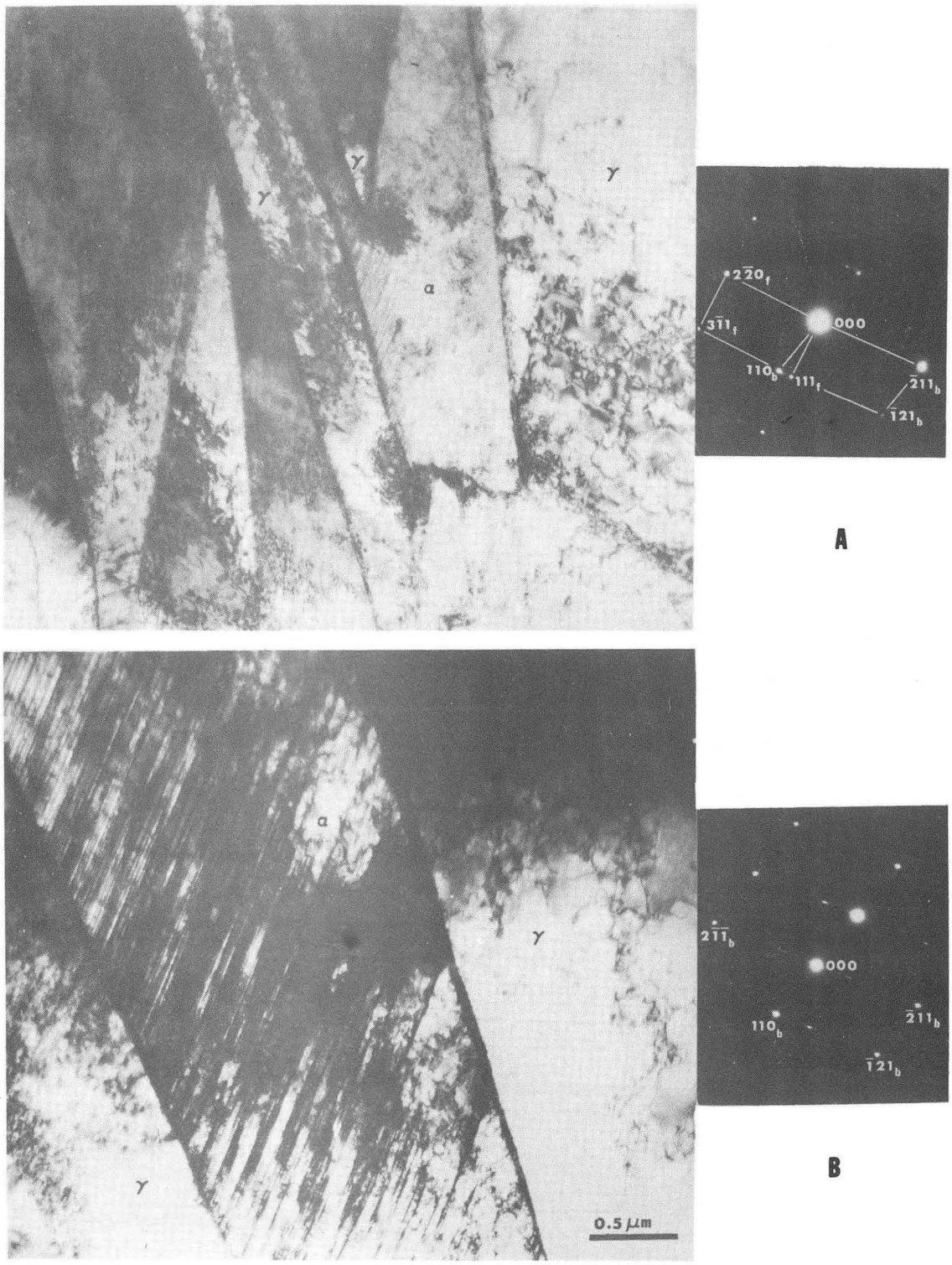

XBB 718-3570

Fig. 22.

LEGAL NOTICE

This report was prepared as an account of work sponsored by the United States Government. Neither the United States nor the United States Atomic Energy Commission, nor any of their employees, nor any of their contractors, subcontractors, or their employees, makes any warranty, express or implied, or assumes any legal liability or responsibility for the accuracy, completeness or usefulness of any information, apparatus, product or process disclosed, or represents that its use would not infringe privately owned rights.

TECHNICAL INFORMATION DIVISION
LAWRENCE BERKELEY LABORATORY
UNIVERSITY OF CALIFORNIA
BERKELEY, CALIFORNIA 94720